Thermodynamic and transport properties of dense hydrogen plasmas

Heidi Reinholz, Ronald Redmer, and Stefan Nagel
Universität Rostock, Fachbereich Physik, Universitätsplatz 3, D-18051 Rostock, Germany
(Received 5 January 1995; revised manuscript received 26 May 1995)

Thermodynamic and transport properties of dense plasmas are expressed by Green's functions within a consistent quantum statistical approach. The equation of state for hydrogen plasma is evaluated within a generalized Beth-Uhlenbeck approach utilizing a quasiparticle picture for the one- and two-particle states. Taking into account also further clusters such as dimers and molecular ions, the stability behavior of the thermodynamic functions is studied with respect to the hypothetical plasma phase transition. The electrical and thermal conductivity, as well as the thermopower, are then calculated within the linear response theory as given by Zubarev. Especially, the effects of arbitrary degeneracy, ion-ion structure factor, screening, and of partial ionization are studied. The interactions between the various species are treated on the T matrix level. The numerical results interpolate between the Spitzer theory for fully ionized, nondegenerate plasmas and the Ziman theory for metallic densities. The plasma phase transition is accompanied by a metal-nonmetal transition, which is characterized by drastic changes of the electronic properties, as can be deduced from the behavior of the transport properties.

PACS number(s): 52.25.−b, 05.60.+w, 51.10.+y

I. INTRODUCTION

We consider a neutral hydrogen plasma consisting of electrons (mass $m_e = m$, charge $q_e = -e$) and protons ($m_p = M$, $q_p = +e$) with $n_e = n_p = n$. In order to characterize the plasma state, we introduce the Coulomb coupling constant Γ for the ion system and the degeneracy parameter Θ for the electron system [1],

$$\Gamma = \frac{(Ze)^2}{4\pi\varepsilon_0 k_B T d}\ , \quad \Theta = \frac{k_B T}{E_F}\ . \tag{1}$$

E_F denotes the Fermi energy, d is the mean distance between the particles, and a_B is the Bohr radius,

$$E_F = \frac{\hbar^2}{2m}(3\pi^2 n)^{2/3}\ , \quad d = \left(\frac{3}{4\pi n}\right)^{1/3}\ , \quad a_B = \frac{4\pi\varepsilon_0\hbar^2}{me^2}\ . \tag{2}$$

This paper is devoted to hydrogen plasma from the nondegenerate, weakly nonideal domain ($\Theta \gg 1$, $\Gamma \leq 1$) up to the degenerate, strongly coupled region ($\Theta \ll 1$, $\Gamma \gg 1$). The physical properties are influenced by many-particle effects. For instance, in the nondegenerate, weakly nonideal domain, dynamic screening and self-energy effects as well as the formation and decay of bound states (atoms H, dimers H_2, molecular ions H_2^+, etc.) are important, whereas in the degenerate, strongly coupled region structure factor and local-field corrections, arbitrary degeneracy, and Pauli blocking are relevant (for a review, see [2]).

The electronic properties show drastic changes when the density is varied. At low densities, the plasma is nearly fully ionized and reasonably well described within the Debye-Hückel theory for the thermodynamic properties and the Spitzer theory for the transport properties. Dense, nonideal plasmas are characterized by partial ionization where bound states strongly affect the physical properties. For instance, the electrical conductivity can have values with $\sigma \leq 10^4/(\Omega\ \mathrm{m})$ for $T \leq 10^4$ K [3], which indicates already a nonmetallic behavior when utilizing the Mott criterion also for plasmas. At very high densities, bound states disappear due to the Mott effect and the plasma becomes fully ionized again. The electrical conductivity is described by the Ziman formula.

Zero-temperature calculations have indicated that a first-order phase transition must occur at high pressures around 150 GPa between the insulating molecular phase and the conducting metallic phase (for a review, see [4]). Electrical conductivities measured in shock compression experiments with fluid molecular hydrogen and deuterium [5] have clearly shown that H_2 and D_2 are semiconducting fluids with an energy gap of about 12 eV.

The corresponding nonmetal-to-metal transition at finite temperatures is usually connected with a thermodynamic phase transition, the up to now hypothetical *plasma phase transition* [6,7]. Especially, the location of a (second) critical point of this plasma phase transition is of high interest with respect to a better understanding of matter at high pressures and temperatures as it is relevant for, e.g., astrophysical systems.

All approaches to the equation of state of strongly coupled plasmas based on the chemical picture that treats elementary species (electrons and protons) as well as composites (atoms, molecules, molecular ions, etc.) on the same footing have resulted in various estimates for that critical point in hydrogen [6–12], helium [13], hydrogen-helium [12,14], and xenon plasma [15].

There, nonideality corrections to the equation of state

are usually considered within the following model: the Coulomb interactions between charged particles beyond the Debye-Hückel theory, the polarization interactions between charged particles and neutrals by means of the second virial coefficient with respect to a polarization potential, and the interaction between neutrals within the framework of extended fluid perturbation theory which gives reasonable results compared with available shock-wave experiments [16] and Monte Carlo simulations [6].

In this paper, a unified approach to the thermodynamic and transport properties of dense plasmas is utilized (for details, see [2,17]). The equation of state takes into account the self-energy of single-particle states within the T matrix approximation [18]. The partition function of correlated two-particle states, a generalized Beth-Uhlenbeck formula [19], consists of a bound and a scattering part. Thus, at least on the two-particle level, the chemical picture has been avoided.

The chemical potential is studied as a function of temperature and density. The thermodynamic stability criterion $(\partial\mu/\partial n)_T \geq 0$ is utilized to locate the critical point of the plasma phase transition. Furthermore, the degree of ionization and the composition of hydrogen plasma are determined.

The transport properties are calculated within linear response theory given here in the formulation of Zubarev [20]. Transport coefficients are expressed by equilibrium correlation functions [3,21,22]. Transport cross sections for the scattering between the various species are calculated on T matrix level. The ion-ion structure factor $S_{ii}(q)$ is determined within the hypernetted chain (HNC) approximation considering also local-field corrections to the dielectric function $\varepsilon(q,\omega)$.

Numerical results for the electrical and thermal conductivity as well as the thermopower are given for a large domain of the density-temperature plane ranging from nondegenerate, weakly nonideal plasmas up to degenerate, strongly coupled plasmas.

There is a close connection to the behavior of expanded fluid alkali-atom metals and mercury which follow the plasma region in the density-temperature plane continuously towards higher densities and lower temperatures. There, the metal-nonmetal transition takes place near the critical point of the liquid-vapor phase transition (for a review, see [23,24]).

II. THERMODYNAMIC PROPERTIES OF HYDROGEN PLASMA

A. Equation of state

In partially ionized plasmas, bound states such as atoms H, dimers H_2, molecular ions H_2^+, H^-, and further clusters are formed out of the elementary particle electrons e and protons p. We take into account clusters up to $N = 4$, i.e., dimers H_2, accordant with [10,11]

$$\begin{aligned} &e+p \rightleftharpoons \mathrm{H}\ , \quad e+\mathrm{H} \rightleftharpoons \mathrm{H}^-\ , \\ &p+\mathrm{H} \rightleftharpoons \mathrm{H}_2^+\ , \quad \mathrm{H}+\mathrm{H} \rightleftharpoons \mathrm{H}_2\ . \end{aligned} \tag{3}$$

The concentration of higher clusters is negligible as can be deduced from respective ideal Saha equations.

The equation of state is derived from the relation between the one-particle density $n_c(\beta,\mu)$ for the species $c = e,p$, and the imaginary part of the thermodynamic Green's function $G_c(\mathbf{k},z)$ — the spectral function — via [17]

$$n_c(\beta,\mu_c) = \frac{1}{\Omega_0}\sum_{\mathbf{k}}\int\frac{d(\hbar\omega)}{\pi}\,\mathrm{Im}\,G_c(\mathbf{k},\omega-i0^+)\,f_c(\hbar\omega)\,, \tag{4}$$

where $\beta = 1/k_BT$ is the inverse temperature, Ω_0 the normalization volume, and μ_c denotes the chemical potential of species $c = e,p$. $f_c(E) = \{\exp[\beta(E-\mu_c)]+1\}^{-1}$ is the Fermi distribution function. The chemical potential $\mu(\beta,n)$ is obtained from Eq. (4) by inversion, whereas the pressure $p(\beta,\mu) = \int_{-\infty}^{\mu} d\bar{\mu}\, n(\beta,\bar{\mu})$ follows after a simple integration.

The Green's function $G_c(\mathbf{k},z)$ is related to the self-energy $\Sigma_c(\mathbf{k},z)$ via the Dyson equation,

$$\begin{aligned} G_c(\mathbf{k},z_\nu)^{-1} &= \hbar z_\nu - E_c(k) - \Sigma_c(\mathbf{k},z_\nu)\ , \\ z_\nu &= i\pi\nu/\beta + \mu_c\ , \quad \nu = \pm1,\pm3,\ldots\ . \end{aligned} \tag{5}$$

z_ν are Matsubara frequencies and $E_c(k) = \hbar^2k^2/2m_c$ is the kinetic energy of free particles. Quasiparticle energies are usually defined by the solution of

$$\varepsilon_c(\mathbf{k}) = E_c(k) + \mathrm{Re}\Sigma_c[\mathbf{k},\varepsilon_c(\mathbf{k})/\hbar + i0]\ . \tag{6}$$

In order to describe the formation of atoms H, dimers H_2, molecular ions H_2^+, H^-, as well as higher-order clusters out of the elementary species e,p, the self-energy (and also the polarization function) have to be decomposed into a sum over the contributions of N-particle ladder T matrices (for details, see [25–27]). These quantities are determined by respective Bethe-Salpeter equations with an effective two-particle interaction kernel that contains the dynamically screened potential and further in-medium corrections to their energy spectrum via the cluster contributions to the polarization function. We consider here the dominant bound state part of the N-particle T matrices with $N \geq 3$. For hydrogen atoms ($N = 2$), also the scattering state part becomes of importance as shown below.

Inserting this cluster expansion into Eq. (4), the total electron density is given by

$$n_e(\beta,\mu_e) = n_e^{(1)} + n_{\mathrm{H}}^{(2)} + n_{\mathrm{H}_2^+}^{(3)} + 2n_{\mathrm{H}_2}^{(4)}\ , \tag{7}$$

where the partial densities are given by respective partition functions.

B. Two-particle partition function

In a first step, molecular ions ($N = 3$) and dimers ($N = 4$) are neglected. Zimmermann and Stolz [18] derived an equation of state from Eq. (4) which is the sum of the density of free quasiparticles, $n_c^{(1)}$, and of a density of correlated two-particle states, $n_{\mathrm{H}}^{(2)}$. Replacing the slightly $\mathbf{k}$-dependent self-energy shift in Eq. (6) by a constant quantity Δ_c, which is fixed by the free quasiparticle density,

$$n_c^{(1)} = \frac{1}{\Omega_0}\sum_{\mathbf{k}} f_c[\varepsilon_c(k)] \ , \quad \varepsilon_c(k) = E_c(k) + \Delta_c \ ,$$
$$\Delta_c = \left\{ \frac{1}{\Omega_0}\sum_{\mathbf{k}} f_c'[\varepsilon_c(k)]\, \mathrm{Re}\,\Sigma_c[\mathbf{k}, \varepsilon_c(k)/\hbar + i0] \right\} \Big/ \left\{ \frac{1}{\Omega_0}\sum_{\mathbf{k}} f_c'[\varepsilon_c(k)] \right\} , \tag{8}$$

and utilizing the optical theorem, a generalized Beth-Uhlenbeck formula [19] can be derived for the correlated density, which reads for the nondegenerate case:

$$n_{\mathrm{H}}^{(2)} = [n_e^{(1)}]^2 \Lambda_{ep}^3 Z_e \ , \quad Z_e = Z_{ep} + 2^{3/2} Z_{ee} \ ,$$
$$Z_{ep} = \sum_\ell (2\ell+1) \left\{ \sum_n [\exp(-\beta\varepsilon_{n\ell}) - 1] + \int_0^\infty dk \left(\frac{\beta\hbar^2 k}{2\mu_{ep}}\right) \exp\left(-\frac{\beta\hbar^2 k^2}{2\mu_{ep}}\right) \frac{2}{\pi} \left[\delta_\ell(k) - \frac{1}{2}\sin[2\delta_\ell(k)]\right] \right\} , \tag{9}$$
$$Z_{ee} = \sum_\ell (2\ell+1) \left(1 - \frac{(-1)^\ell}{2}\right) \int_0^\infty dk \left(\frac{\beta\hbar^2 k}{2\mu_{ee}}\right) \exp\left(-\frac{\beta\hbar^2 k^2}{2\mu_{ee}}\right) \frac{2}{\pi} \left[\delta_\ell(k) - \frac{1}{2}\sin[2\delta_\ell(k)]\right] .$$

$n_c^{(1)} = 2\Lambda_c^{-3} \exp[-\beta(\Delta_c - \mu_c)]$ is the quasiparticle density. $\Lambda_c = (2\pi\beta\hbar^2/m_c)^{1/2}$ denotes the thermal wavelength, and μ_{ed} is the reduced mass ($d = e, p$).

The correlated two-particle density consists of the sum over the discrete bound state energies $\varepsilon_{n\ell}$ and the integral over the continuous scattering states, characterized by their scattering phase shifts $\delta_\ell(k)$. Utilizing the Levinson theorem [28], the first expansion term of the bound state part with respect to $\beta\varepsilon_{n\ell}$ was projected into the scattering state part. The additional term $\sin[2\delta_\ell(k)]$ in the scattering state part compared with the standard Beth-Uhlenbeck formula results from the definition of the quasiparticle density $n_c^{(1)}$ via the full self-energy shift Δ_c [18]. The discontinuities in the bound state part, which occur whenever a bound state disappears due to screening effects, are compensated by respective contributions in the scattering state part and the whole partition function, Eq. (9), remains a smooth function.

Performing another integration by parts in Eq. (9), the finite Planck-Larkin partition function is obtained for the first, bound state part of the full two-particle partition function (see also [29]),

$$Z_{ep}^{\mathrm{PL}} = \sum_\ell (2\ell+1) \sum_n [\exp(-\beta\varepsilon_{n\ell}) - 1 + \beta\varepsilon_{n\ell}] \ . \tag{10}$$

Although (10) describes only bound state contributions to the thermodynamic functions, the Planck-Larkin convention has frequently been used for the two-particle partition function of low-temperature plasmas where scattering states can be neglected [8,9,15,25,27,30]. This treatment is appropriate for, e.g., low-temperature alkali-atom plasmas.

For hydrogen and also inert gas plasmas such as xenon, the situation is more involved. For comparison, we have calculated the two-particle partition function $Z_e = Z_{ep} + 2^{3/2} Z_{ee}$, Eq. (9), for the Debye potential

$$V_{ed}(r) = \frac{q_e q_d}{4\pi\varepsilon_0 r} \exp(-r/R_D) \ . \tag{11}$$

The screening length R_D is given for arbitrary electron degeneracy by

$$\frac{1}{R_D^2} = \frac{\beta e^2}{4\pi\varepsilon_0} \frac{2}{\Lambda_e^3} I_{-1/2}(\beta\mu_e^{id}) \ . \tag{12}$$

Free particle density and ideal part of the chemical potential are connected via the relation $n_c\Lambda_c^3/2 = I_{1/2}(\beta\mu_c^{id})$. $I_n(x)$ are Fermi integrals. We consider the heavy protons rather producing a microfield distribution in the plasma than contributing to the static screening length. From a study of dynamic screening effects on the collision integrals [31] one can conclude that static screening of electrons *and* protons overestimates screening effects considerably so that Eq. (12) is more appropriate.

The bound state energies $\varepsilon_{n\ell}$ and scattering phase shifts δ_ℓ were determined by solving the Schrödinger equation for the attractive or repulsive Debye potential (11) numerically. The respective values were checked against earlier results [32–34]. The results for the Planck-Larkin, the standard Beth-Uhlenbeck, and the modified Zimmermann-Stolz partition functions are compared in Table I for given temperatures and inverse screening lengths $\kappa = 1/R_D$.

All three partition functions are smooth functions with respect to the density so that no unphysical jumps in the thermodynamic functions occur whenever a bound state vanishes. Furthermore, the bound state part dominates the partition function for low temperatures, i.e., $T \leq 2\times10^4$ K, and screening parameters $\kappa a_B \leq 0.5$. The scattering state contribution is not negligible for larger screening parameters κa_B where only a small number of bound states remains and compensation effects between bound and scattering contributions are considerable. For higher temperatures and low densities, the number of scattering states increases strongly so that their contribution to the two-particle partition function becomes dominant.

The discrepancies between the standard Beth-Uhlenbeck and the Zimmermann-Stolz partition function are small for low temperatures. For the low and high density limit, however, pronounced deviations occur which are due to the utilization of the quasiparticle picture by Zimmermann and Stolz [18].

To study the influence of two-particle scattering states

on the thermodynamic functions, the Planck-Larkin and Zimmermann-Stolz partition functions are inserted into the law of mass action, $e + p \rightleftharpoons \mathrm{H}$. The Planck-Larkin convention (10) may serve as the simplest version of the chemical picture, while the quasiparticle picture of Zimmermann and Stolz contains at least the full two-particle partition function for the nondegenerate case.

TABLE I. Values for the two-particle partition function for the Debye potential (11) for various inverse screening lengths $\kappa = 1/R_D$ and temperatures T. Z_{ep}^{PL} denotes the Planck-Larkin partition function (10), Z_e^{BU} is the standard Beth-Uhlenbeck result (without the sine term), and Z_e^{ZS} is the Zimmermann-Stolz partition function according to (9). The notation 0.1352 [+2] stands for $0.1352 \times 10^{+2}$.

κa_B	Z_{ep}^{PL}	Z_e^{BU}	Z_e^{ZS}
	$T = 10 \times 10^3$ K		
2.00	0.00	0.6602 [−1]	0.3386 [−2]
1.25	0.00	0.3398 [+0]	0.2314 [+0]
1.00	0.5896 [−1]	0.1009 [+1]	0.1127 [+1]
0.67	0.9908 [+1]	0.1336 [+2]	0.1352 [+2]
0.50	0.1018 [+3]	0.1073 [+3]	0.1075 [+3]
0.40	0.5182 [+3]	0.5255 [+3]	0.5255 [+3]
0.25	0.9756 [+4]	0.9767 [+4]	0.9768 [+4]
0.10	0.3823 [+6]	0.3824 [+6]	0.3824 [+6]
0.05	0.1571 [+7]	0.1571 [+7]	0.1571 [+7]
0.01	0.5260 [+7]	0.5260 [+7]	0.5260 [+7]
	$T = 20 \times 10^3$ K		
2.00	0.00	0.8192 [−1]	0.6689 [−2]
1.25	0.00	0.3313 [+0]	0.2326 [+0]
1.00	0.1393 [−1]	0.7237 [+0]	0.8111 [+0]
0.67	0.1374 [+1]	0.3386 [+1]	0.3546 [+1]
0.50	0.7028 [+1]	0.1021 [+2]	0.1033 [+2]
0.40	0.1879 [+2]	0.2301 [+2]	0.2306 [+2]
0.25	0.9323 [+2]	0.1001 [+3]	0.1006 [+3]
0.10	0.6124 [+3]	0.6295 [+3]	0.6319 [+3]
0.05	0.1251 [+4]	0.1285 [+4]	0.1292 [+4]
0.01	0.2302 [+4]	0.2502 [+4]	0.2656 [+4]
	$T = 30 \times 10^3$ K		
2.00	0.00	0.9041 [−1]	0.9287 [−2]
1.25	0.00	0.3209 [+0]	0.2261 [+0]
1.00	0.6078 [−2]	0.6174 [+0]	0.6832 [+0]
0.67	0.5139 [+0]	0.2044 [+1]	0.2191 [+1]
0.50	0.2195 [+1]	0.4575 [+1]	0.4698 [+1]
0.40	0.4982 [+1]	0.8129 [+1]	0.8211 [+1]
0.25	0.1731 [+2]	0.2255 [+2]	0.2308 [+2]
0.10	0.6789 [+2]	0.8144 [+2]	0.8395 [+2]
0.05	0.1126 [+3]	0.1408 [+3]	0.1484 [+3]
0.01	0.1741 [+3]	0.3552 [+3]	0.5493 [+3]
	$T = 50 \times 10^3$ K		
2.00	0.00	0.9910 [−1]	0.1298 [−1]
1.25	0.00	0.3020 [+0]	0.2111 [+0]
1.00	0.2156 [−2]	0.5169 [+0]	0.5550 [+0]
0.67	0.1625 [+0]	0.1296 [+1]	0.1415 [+1]
0.50	0.6129 [+0]	0.2338 [+1]	0.2450 [+1]
0.40	0.1247 [+1]	0.3530 [+1]	0.3628 [+1]
0.25	0.3442 [+1]	0.7268 [+1]	0.7837 [+1]
0.10	0.9704 [+1]	0.2002 [+2]	0.2284 [+2]
0.05	0.1418 [+2]	0.3640 [+2]	0.4574 [+2]
0.01	0.1995 [+2]	0.1917 [+3]	0.4300 [+3]

C. Formation of clusters

In a next step, besides hydrogen atoms also dimers and molecular ions are considered. Saumon and Chabrier [6,7] found dimer fractions up to 95% near the plasma phase transition, whereas Haronska, Kremp, and Schlanges [11] extracted dimer fractions up to 70% from their calculations. Substantial concentrations of dimers A_2 and molecular ions $A_2{}^+$ were also obtained near the critical point of the liquid-vapor phase transition in hydrogenlike expanded alkali-atom fluids and plasmas, where a metal-nonmetal transition takes place [25,30,35,36].

The formation of molecular ions, $p + \mathrm{H} \rightleftharpoons \mathrm{H_2}^+$, and of dimers, $2\mathrm{H} \rightleftharpoons \mathrm{H_2}$, can be described by respective laws of mass action,

$$n_{\mathrm{H_2}^+}^{(3)} = n_{\mathrm{H}}^{(2)} n_p K_{\mathrm{H_2}^+} \ , \quad n_{\mathrm{H_2}}^{(4)} = [n_{\mathrm{H}}^{(2)}]^2 K_{\mathrm{H_2}} \ . \tag{13}$$

The quantities K are given by the partition functions of the species involved in the reaction and reduce to the well-known Saha equations only in the low-density limit. For arbitrary densities, the K's become dependent on density and temperature. Due to the condition of charge neutrality, the various mass action laws are not independent from each other and we have finally a coupled, strongly nonlinear system of equations,

$$[n_e^{(1)}]^2 Z_e = n_{\mathrm{H}}^{(2)} [1 + n_{\mathrm{H}}^{(2)} K_{\mathrm{H_2}^+}] \ . \tag{14}$$

D. Quasiparticle shifts and partition functions

The mass action laws, Eqs. (9) and (13), are solved by inserting appropriate expressions for the quasiparticle shifts and the partition functions for atoms H, dimers $\mathrm{H_2}$, and molecular ions $\mathrm{H_2}^+$. Considering the definition of the quasiparticle density, Eq. (8), and the relation between the ideal part of the chemical potential and the free particle density, $n_c \Lambda_c^3/2 = I_{1/2}(\beta \mu_c^{id})$, the shifts Δ_c can also be interpreted as the interaction parts of the chemical potential,

$$\mu_c = \mu_c^{id} + \mu_c^{\mathrm{int}} \ , \quad \mu_c^{\mathrm{int}} = \Delta_c \ . \tag{15}$$

The shifts Δ_c can be decomposed into the Hartree-Fock (HF) and Montroll-Ward (MW) contributions, characterizing the self-energy of charged particle interactions in second order with respect to the screened Coulomb potential, and a polarization contribution (PP) that is due to interactions between charged particles and neutral bound states,

$$\Delta_c = \Delta_c^{\mathrm{HF}} + \Delta_c^{\mathrm{MW}} + \Delta_c^{\mathrm{PP}} \ . \tag{16}$$

For simplicity, we have used the Padé approximations of Ebeling and Richert [8,9] for the charged particle

self-energy, $\Delta_c^{\rm HF} + \Delta_c^{\rm MW} \equiv \mu_c^{\rm gas}$, which interpolate between the known limiting cases of nondegeneracy (Debye-Hückel theory), the strong-coupling limit for the electrons (Gell-Mann and Brueckner result [37]), and the case of strongly correlated ions (Madelung energy). Thus, these formulas cover the whole density region from the dilute plasma to the dense fluid state within an estimated maximum error of about 20% [38].

The polarization contribution $\Delta_c^{\rm PP}$ was calculated for arbitrary densities for the interaction of electrons with hydrogen atoms [39]. The results can be given in a parametrized form as linearized virial coefficients $B_{e,A}^{\rm PP}$ with respect to a local polarization potential $V^{\rm PP}(R)$ [27],

$$\Delta_e^{\rm PP} = n_H^{(2)} B_{e,H}^{\rm PP} \ , \quad B_{e,H}^{\rm PP} = \int d^3R \, V^{\rm PP}(R) \ , \qquad (17)$$

$$V^{\rm PP}(R) = -\frac{e^2 \alpha_D \exp(-2\kappa R)}{2(4\pi\varepsilon_0)^2 (R^2 + r_0^2)^2} (1 + \kappa R)^2 \ .$$

The values for the dipole polarizability α_D and the cutoff radius r_0 are given in Table II. $\kappa = 1/R_D$ is the inverse screening length.

The energy spectrum of atoms is shifted due to the interaction with free quasiparticles (PP) as well as with other atoms and clusters [van der Waals (vdW)]

$$\varepsilon_{n\ell} = E_{n\ell} + \Delta E_{n\ell} \ , \ \Delta E_{n\ell} = \Delta E_{n\ell}^{\rm PP} + \Delta E_{n\ell}^{\rm vdW} \ . \qquad (18)$$

These terms can be derived from in-medium corrections to the Bethe-Salpeter equation (see, e.g., [25,26,39]). We have taken into account these energy shifts in form of a correction factor in the two-particle partition function, Eq. (9), via $Z_e^{\rm eff} = Z_e \exp(\Delta E_{n\ell})$, supposing that the total correlated two-particle density reacts like that of hydrogen atoms which, of course, overestimates these contributions.

The polarization contribution is given by $\Delta E_{n\ell}^{\rm PP} = n_e^{(1)} B_{e,H}^{\rm PP}$ similar to Eq. (17). The second, van der Waals term describes the long-range attraction between neutrals as well as the short-range repulsion between clusters. For these terms, the density and temperature dependent interaction potentials between H, H_2, and $H_2{}^+$ have to be known for arbitrary distances in order to calculate, e.g., the respective virial coefficients. This complex problem has only been solved approximately up to now which is the source of substantial uncertainties in the various theories. Utilizing extended fluid perturbation theory [6,7] yields reasonable agreement with results of shock-wave experiments [16] and Monte Carlo simulations.

Within the van der Waals two-fluid theory [40], the intermolecular potentials are replaced by effective, temperature-dependent hard-core radii so that the respective well-known expressions for the thermodynamic functions of a hard-core reference system can be applied (see, e.g., [11]).

We have chosen here the interatomic H-H potential derived by Aviram, Goshen, and Thieberger [41] and then calculated an effective hard-core radius by means of the Barker-Henderson theory [40]. With this value and the known equilibrium distances in the hydrogen dimer H_2 and the molecular ion $H_2{}^+$, effective hard-core radii can also be derived for these species. The respective contribution (vdW) in Eq. 18) is then given by a modified Carnahan-Starling-type expression derived by Mansoori *et al.* [42] for the chemical potential of a mixture of hard spheres, $\Delta E_{n\ell}^{\rm vdW} \equiv \mu_{\rm H}^{\rm HC}$.

The mass action laws for the dimers and molecular ions, Eqs. (13), contain the partition functions $K_{\rm H_2}$ and $K_{\rm H_2{}^+}$, respectively, which are treated in the usual way by separating the internal quantum numbers with respect to the translational, spin, electronic, rotational, and vibrational degrees of freedom,

$$K_{{\rm H}_N} = \Lambda_{{\rm H}_N}^{-3} \, \sigma_{{\rm H}_N}^{\rm spin} \, \sigma_{{\rm H}_N}^{\rm el} \, \sigma_{{\rm H}_N}^{\rm rot} \sigma_{{\rm H}_N}^{\rm vib} \ . \qquad (19)$$

These terms are given by

TABLE II. Paramaters for the calculation of the chemical equilibria in hydrogen plasma.

Parameter		
Polarizability $\alpha_{\rm H}$ in a_B^3		4.5[a]
Cutoff radius r_0 in a_B		1.4565[a]
Effective atomic radius $R_{\rm H}$ in a_B	1.10[b]	($T = 10 \times 10^3$ K)
	1.00[b]	($T = 15 \times 10^3$ K)
	0.91[b]	($T = 20 \times 10^3$ K)
Equilibrium distance $d_{\rm H_2{}^+}$ in a_B		2.00[c]
Equilibrium distance $d_{\rm H_2}$ in a_B		1.40[c]
$D_{\rm H_2}$ of dimers in eV		4.75[c]
$D_{\rm H_2{}^+}$ of molecular ions in eV		2.79[c]
Rotational constant of dimers $B_{\rm H_2}$ in cm^{-1}		60.8[c]
Rotational constant of molecular ions $B_{\rm H_2{}^+}$ in cm^{-1}		29.8[c]
Vibrational frequency of dimers $\omega_{\rm H_2}$ in cm^{-1}		4395[c]
Vibrational frequency of molecular ions $\omega_{\rm H_2{}^+}$ in cm^{-1}		2297[c]

[a]Redmer, Röpke, and Zimmermann [39].

[b]Effective hard-core radii within the Barker-Henderson method [40]; see also Haronska, Kremp, and Schlanges [11].

[c]See, for instance, B.H. Bransden and C.J. Joachain, *Physics of Atoms and Molecules* (Longman Scientific & Technical, New York, 1983), p. 393.

$$\sigma_{H_N}^{el} = \exp(\beta D_{H_N} + \Delta E_{H_N}) ,$$
$$\sigma_{H_N}^{rot} = \beta hc/B_{H_N} , \qquad (20)$$
$$\sigma_{H_N}^{vib} = \left[1 - \exp\left(-\frac{\omega_{H_N}}{\beta hc}\right)\right]^{-1} ,$$

where B_{H_N}, ω_{H_N}, and D_{H_N} are the characteristic rotational constant, the vibrational frequency, and the dissociation energy of molecular ions ($N = 3$) and dimers ($N = 4$), respectively. c is the speed of light.

We have taken into account interaction corrections to these mass action laws via quantities ΔE_{H_N} similar to the case of atoms. Comparing the dipole polarizabilities of hydrogen atoms and dimers [43], $f = \alpha_{H_2}/\alpha_H$, one finds $f \approx 1.23$ which is utilized as a scaling factor for the respective virial coefficient, $B_{e,H_2}^{PP} \approx f \times B_{e,H}^{PP}$. Effective hard-core radii for the dimers and molecular ions have been derived from the effective atomic radius and the equilibrium distances in these clusters as described above, so that $\Delta E_{H_N} = \mu_{H_N}^{HC}$. The parameters that are necessary for the evaluation of the respective formulas are given in Table II.

E. Composition of hydrogen plasma

We have displayed the composition of hydrogen plasma in Fig. 1 for a given temperature as function of the density. We can clearly distinguish between three different regions. The low-density plasma is weakly ionized with an ionization degree of less than 5% and extends up to about 10^{23} cm^{-3}. It consists mainly of atoms H and dimers H_2, the latter reaching a maximum concentration of about 90% for $T = 10\times10^3$ K and 70% for $T = 15\times10^3$ K at about this density. Dimers are not negligible in the region above 10^{19} cm^{-3}.

The second region from 10^{23} cm^{-3} up to 2×10^{24} cm^{-3} is characterized by partial ionization from 5% to 80%.

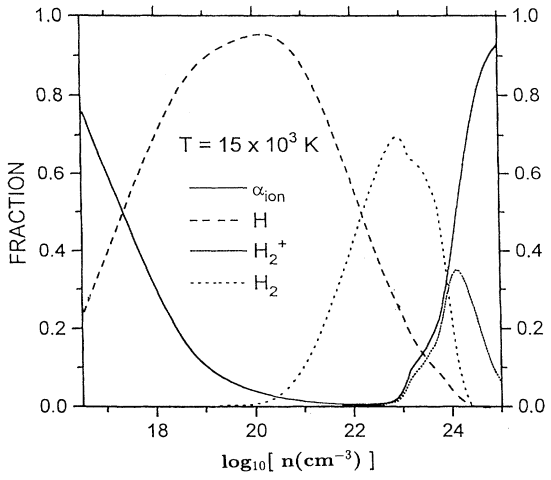

FIG. 1. Composition of hydrogen plasma for $T = 15 \times 10^3$ K as a function of the particle number density n. The fraction of free electrons e, atoms H, dimers H_2, and molecular ions H_2^+ is shown.

Here, all species have strongly varying concentrations, which is a result of the nonideality corrections to the mass action laws. Dimers vanish at about 2×10^{24} cm^{-3}, where molecular ions H_2^+ reach their maximum concentration of about 35%. Then, the ionization degree is sharply rising with increasing densities, which is a result of pressure ionization (Mott effect).

Hummer and Mihalas [44] found a maximum concentration for molecular ions H_2^+ of only 6.2×10^{-4} in nearly the same density-temperature region within a free-energy minimization scheme for the coupled chemical equilibria. This discrepancy is possibly caused by the use of different parameters for the internal partition functions, and the simple neutral-neutral interaction for the evaluation of the occupation probabilities performed by Hummer and Mihalas. The latter forces pressure dissociation of H_2 for $\varrho \approx 0.1$ g/cm^3 at arbitrary temperatures.

The third region above 2×10^{24} cm^{-3} is nearly fully ionized and completely described by the degenerate electron gas immersed in the positive background of protons and molecular ions. For high-temperature plasmas with $T \geq 50 \times 10^3$ K, the fraction of neutral and charged clusters is decreasing, and we have simply a three-component system of electrons, protons, and hydrogen atoms that is reasonably well described within an extended Debye-Hückel theory [45].

F. Plasma phase transition

The chemical potential of hydrogen plasma,

$$\mu_{plasma} \equiv \mu_e + \mu_p = \mu_e^{id} + \mu_p^{id} + \mu_e^{gas} + \mu_p^{gas} + \left(n_H^{(2)} + f n_{H_2}^{(4)}\right) B_{e,H} + \mu_H^{HC} , \qquad (21)$$

is shown in Fig. 2 for $T = (10, 15, 20) \times 10^3$ K within three different models. The ideal part of the chemical potential is always calculated for arbitrary degeneracy via the Fermi integral. The electron and proton gas contributions are taken in the parametrized form of Ebeling and Richert [8,9].

The simplest model (a) (dash-dotted line) considers only electrons, protons, and hydrogen atoms the fraction of which was determined by means of the Planck-Larkin partition function (10). Dimers and molecular ions were neglected. Furthermore, the hard-core contributions that might be the source of substantial uncertainties at high densities are also neglected.

Molecular ions and dimers as well as the respective hard-core contributions have been included in model (b) (dashed line). In case (c) (solid line), the Planck-Larkin partition function was replaced by the Zimmermann-Stolz two-particle partition function (9) so that the influence of scattering states is included. All other contributions are the same as in case (b).

The resulting curves for the chemical potential indicate that a thermodynamic instability occurs in all three models. The instability is inherent already in the simplest model (a) and, therefore, produced by the electron and

proton gas contributions to the chemical potential, which were taken from Ebeling and Richert [8,9]. Not surprisingly, the results for the critical point of the plasma phase transition within this model coincide very well with their estimates. We find $T_c = 15 \times 10^3$ K, $\rho_c = 0.2$ g/cm^3, and $p_c = 26$ GPa compared with their data, $T_c = 16.5 \times 10^3$ K, $\rho_c = 0.13$ g/cm^3, and $p_c = 23$ GPa.

The consideration of molecular ions and dimers as well as of effective intermolecular interactions in model (b) changes the results only slightly between $\log_{10}(n \times \mathrm{cm}^3) = 22.5 - 23.5$. The instability region is now smaller and shifted towards higher densities, indicating that the consideration of further neutrals (dimers) tends to *stabilize* the system. This is a result of the polarization contributions $B_{e,\mathrm{H}}$ and, especially, B_{e,H_2} in the laws of mass action, which force the ionization degree towards the value $\alpha_{\mathrm{ion}} = 0.5$. In the region of the Mott effect, where α_{ion} increases sharply, these terms yield a smoother transition. Furthermore, the small discrepancies between the results of model (a) and (b) for high densities indicate that the influence of the effective intermolecular interactions on the location of the plasma phase transition is surprisingly small.

The strong influence of two-particle scattering states on the thermodynamic properties at high densities is seen from curve (c). Here, instead of the Planck-Larkin partition function (10), the correlated two-particle density $n_{\mathrm{H}}^{(2)}$ (9) was taken into account. The consideration of two-particle scattering states tends to *enlarge* the instability region compared with model (b). This behavior is an effect of the smoother decrease of Z_e^{ZS} at high densities compared with Z_{ep}^{PL}; see Table I. As a result, the concentration of atoms H, dimers H_2, as well as of molecular ions $H_2{}^+$ decreases gradually at high densities (see Fig. 1) so that these species contribute to the chemical potential up to higher densities. As a further consequence, the strong increase of the chemical potential in the high-density limit occurs only at higher densities where the effective intermolecular interactions already become important.

For the critical point of the plasma phase transition within model (c), we can give the estimate $T_c = 16.5 \times 10^3$ K, $\rho_c = 0.42$ g/cm^3, and $p_c = 57$ GPa, which is in very good agreement with data given recently by Saumon and Chabrier [7], $T_c = 15.3 \times 10^3$ K, $\rho_c = 0.35$ g/cm^3, and $p_c = 61.4$ GPa. In Table III, we review various results for the critical point of the plasma phase transition in hydrogen.

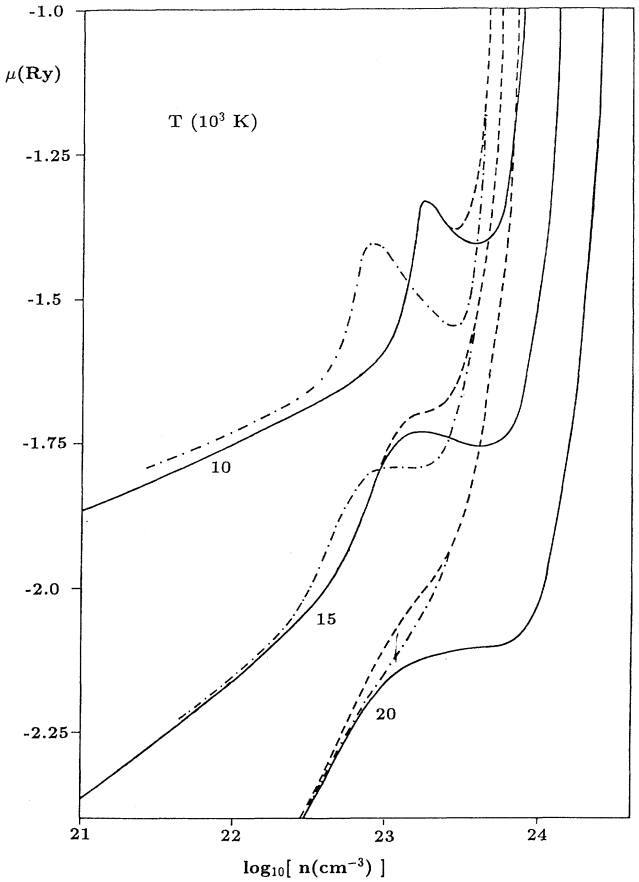

FIG. 2. Chemical potential μ of hydrogen plasma for $T = (10, 15, 20) \times 10^3$ K within three different models (see Sec. II B). Dash-dotted line (a): using the Planck-Larkin partition function (10) and neglecting clusters; dashed line (b): considering clusters H_2, $H_2{}^+$ in addition; solid line (c): using the correct two-particle partition function (9) and considering clusters.

We have treated here at least the correlated two-particle density within a physical picture so that scattering states are included. In order to describe also dimers and molecular ions, the chemical picture was utilized

TABLE III. Theoretical results for the critical point of the hypothetical plasma phase transition in hydrogen. Methods: PIP: partially ionized plasma model; FIT: estimates based on empirical rules.

T_c (in 10^3 K)	p_c (GPa)	ρ_c (g/cm^3)	Method	Reference
19.0	24	0.14	PIP	Robnik and Kundt [10]
16.5	22.5	0.13	PIP	Ebeling and Richert [9]
16.5	95	0.43	PIP	Haronska, Kremp, and Schlanges [11]
15.8	194	1.48	FIT	Hess and Ebeling [46]
15.0	64.6	0.36	PIP	Saumon and Chabrier [6]
15.3	61.4	0.35	PIP	Saumon and Chabrier [7]
14.9	72.3	0.29	PIP	Schlanges, Bonitz, and Tschttschjan [12]
16.5	57	0.42	PIP	Present paper

again. Consistent results for the plasma phase transition should be based on a unified description. However, also other effects may have considerable influence on the thermodynamic properties of strongly coupled hydrogen plasma so that the question whether or not the plasma phase transition is a consequence of utilizing the chemical picture cannot be decided. For instance, the equations of state (7) and (8) have to be evaluated for arbitrary degeneracy considering also Pauli blocking terms. The self-energy should be determined within (off-shell) the T matrix approximation. Furthermore, the effects of band structure and the variation of the internal partition functions with density (e.g., vibron shift) have to be treated, which goes beyond the present approach.

III. THERMOELECTRIC TRANSPORT COEFFICIENTS

A. Linear response method

Electrical conductivity σ, thermopower α, and thermal conductivity λ are well known for nondegenerate, low-density plasmas where the Spitzer theory [47] applies. For strongly degenerate systems such as fluid metals, the Ziman theory is applicable [48] and the electrical conductivity is given by the Ziman formula, the thermopower by the Mott formula, and the thermal conductivity by the Wiedemann-Franz relation.

Most of the theoretical attempts to describe the (electrical and thermal) conductivity of plasmas in a large density-temperature domain are based upon the Ziman formula which is, strictly speaking, only valid for the case of strongly coupled ions and degenerate electrons. Improvements account for many-particle effects such as, for instance, structure factor, local-field corrections, and arbitrary degeneracy [49–52]. On the other hand, improvements of the Spitzer theory have been proposed for the nondegenerate region of strongly coupled, partially ionized [53–56], as well as weakly nonideal [57–59] plasmas. Lee and More [60] evaluated the complete set of transport coefficients for electron transport in electric *and* magnetic fields within a relaxation time approximation for a quantum transport (Boltzmann) equation for arbitrary degeneracy as well as partial ionization.

A general approach to the thermoelectric transport properties of Coulomb systems valid for arbitrary degeneracy has been derived within linear response theory, given here in an extended version originally developed by Zubarev [20] for mechanical and nonmechanical perturbations of an open system (for a review, see [61]). Due to the relation between transport coefficients, correlation functions and thermodynamic Green's functions [3,21,22], this efficient method allows for the treatment of many-particle effects and the consistent inclusion of the composition, as determined in the last section. We will give the main results very briefly, before discussing the transport coefficients in more detail.

The electrical conductivity σ, thermopower α, and thermal conductivity λ are connected with the Onsager transport coefficients L_{ik} [62] according to

$$\sigma = e^2 L_{11} , \quad \alpha = \frac{1}{eT}\frac{L_{12}}{L_{11}} , \qquad (22)$$
$$\lambda = \frac{1}{T}\left(L_{22} - \frac{L_{12}L_{21}}{L_{11}}\right) .$$

Postulating a linear response of the systems with respect to the external forces, electric field, and temperature gradient, the transport coefficients L_{ik} are given in a determinant representation [3,63], known also from standard kinetic theory,

$$L_{ik} = -\frac{(-h)^{i+k-2}}{\Omega_0\,|d|}\begin{vmatrix} 0 & \frac{k-1}{\beta\hbar}\bar{N}_1 - \bar{N}_0 \\ \frac{i-1}{\beta\hbar}N_1 - N_0 & d \end{vmatrix} , \qquad (23)$$

with

$$\bar{N}_m = (\ \bar{N}_{m0}\bar{N}_{m1}\cdots\bar{N}_{mL}\ ) , \qquad (24)$$

$$N_m = \begin{pmatrix} N_{0m} \\ N_{1m} \\ \vdots \\ N_{Lm} \end{pmatrix} , \qquad (d) = \begin{pmatrix} d_{00} & d_{01} & \cdots & d_{0L} \\ d_{10} & d_{11} & \cdots & d_{1L} \\ \vdots & \vdots & \ddots & \vdots \\ d_{L0} & d_{L1} & \cdots & d_{LL} \end{pmatrix} ,$$

where h is the enthalpy per particle.

The correlation functions for thermodynamic equilibrium,

$$\bar{N}_{nm} = N_{nm} + \frac{1}{m}\langle \mathbf{P}_n(\varepsilon); \dot{\mathbf{P}}_m\rangle ,$$
$$N_{nm} = \frac{1}{m}(\mathbf{P}_n, \mathbf{P}_m) , \qquad (25)$$
$$d_{nm} = \langle \dot{\mathbf{P}}_n(\varepsilon); \dot{\mathbf{P}}_m\rangle , \quad \dot{\mathbf{P}}_n = \frac{i}{\hbar}[H_S, \mathbf{P}_n] ,$$

are defined by

$$(A, B) = \int_0^\beta d\tau\, \mathrm{Tr}\{\rho_0\, A(-i\hbar\tau)\, B\} ,$$
$$\langle A(\varepsilon); B\rangle = \lim_{\varepsilon\to 0}\int_{-\infty}^0 dt\, e^{\varepsilon t}\ [A(t), B] , \qquad (26)$$
$$A(t) = e^{iH_S t/\hbar}\, A(0)\, e^{-iH_S t/\hbar},$$
$$\varrho_0 = \frac{1}{Z_0}\exp\left[-\beta H_S + \beta\sum_c \mu_c N_c\right] .$$

The generalized momenta $\mathbf{P}_n$ of the electron system,

$$\mathbf{P}_n = \sum_{\mathbf{k}} \hbar\mathbf{k}[\beta E_e(k)]^n a_e^\dagger(k) a_e(k) , \qquad (27)$$

are a set of relevant observables, which characterize the nonequilibrium state. The terms of lowest order have the physical meaning of electron momentum ($\mathbf{P}_0$) and of the ideal part of the electron energy current ($\mathbf{P}_1$). They are connected with the microscopic expressions for the electrical current density and the electronic heat current density, respectively.

The transport coefficients can be calculated by evaluating the equilibrium correlation functions (25) for arbitrary degeneracy of the system so that we are able to

describe the entire region from nondegenerate, weakly coupled plasmas to degenerate, strongly coupled plasmas.

B. Evaluation of the correlation functions

Neglecting the terms $\langle \mathbf{P}_n(\varepsilon); \dot{\mathbf{P}}_m \rangle$, which are related to the Debye-Onsager relaxation effect, the generalized particle numbers N_{nm} in Eq. (25) are given by Fermi integrals $I_n(x)$,

$$\bar{N}_{nm} = N_{nm} = N_e \frac{\Gamma(n+m+5/2)}{\Gamma(5/2)} \frac{I_{n+m+1/2}(\beta\mu_e^{id})}{I_{1/2}(\beta\mu_e^{id})} , \tag{28}$$

which were evaluated for given densities and temperatures.

The force-force correlation functions d_{nm} are related to four-particle Green's functions via (for details, see [3,21,22])

$$\begin{aligned} d_{nm} &= -\lim_{\varepsilon\to 0} \int_{-\infty}^{0} dt \exp(\varepsilon t) \int_0^\beta d\tau \sum_d \sum_{kpq} \sum_{k'p'q'} V_{ed}(q) V_{de}(q') K_n(k,q) K_m(k',q')\, F(kpq, k'p'q'; t - i\hbar\tau) ; \\ K_n(k,q) &= \mathbf{k}[\beta E_e(k)]^n - (\mathbf{k}+\mathbf{q})[\beta E_e(k+q)]^n ; \\ F(kpq, k'p'q'; t) &= -\int_{-\infty}^{\infty} \frac{d\omega}{2\pi i} \frac{\exp(i\omega t/\hbar)}{\exp(\beta\omega)-1} \left[G_4(\omega + i\varepsilon) - G_4(\omega - i\varepsilon) \right] . \end{aligned} \tag{29}$$

The four-particle Green's functions can be evaluated in terms of Feynman diagrams. The *polarization approximation* describes the interaction of free particles with a system of scatterers in the first Born approximation that is characterized by the dielectric function $\varepsilon(q,\omega)$ (for details, see [21]),

$$\begin{aligned} d_{nm}^{\mathrm{pol}} &= 2\pi\beta\hbar \sum_{k,q} e_k^2 V(q) \int_{-\infty}^{\infty} \frac{d\omega}{\pi} \mathrm{Im}\, \varepsilon^{-1}(q, \omega + i0) \left[1 + g(\omega)\right] \\ &\quad \times f_e(k)[1 - f_e(k+q)]\, K_n(k,q)\, K_m(k+q,-q)\, \delta[\omega + E_e(k+q) - E_e(k)] . \end{aligned} \tag{30}$$

$g(\omega) = [\exp(\beta\omega) - 1]^{-1}$ is the Bose distribution function. The dielectric function $\varepsilon(q,\omega)$ relates the dynamically screened potential $V^s(q,\omega)$ to the polarization function $\Pi(q,\omega)$ according to

$$V_{cd}^s(q,z) = \frac{V_{cd}(q)}{\varepsilon(q,z)} = \frac{V_{cd}(q)}{1 - \sum_{a,b} V_{ab}(q)\Pi_{ab}(q,z)} . \tag{31}$$

A cluster decomposition is employed for the polarization function similar to that for the self-energy Σ, i.e., $\Pi(q,z) = \Pi_1(q,z) + \Pi_2(q,z) + \cdots$ (see Sec. II A), Π_1 represents the RPA for free-particle states, whereas Π_2 describes the contribution of two-particle states to the polarization function [64]. The correlation functions d_{nm} can then be separated with respect to electron-ion, electron-electron, and electron-atom scattering, i.e., $d_{nm} = D_{nm}^{ei} + D_{nm}^{ee} + D_{nm}^{ea}$. The electron-electron and electron-ion contributions have the structure of Lenard-Balescu collision terms with respect to the relevant interaction potentials (see [3]),

$$\begin{aligned} D_{nm}^{\mathrm{ee}} &= \pi\beta\hbar/2 \sum_{k,p,q} \int_{-\infty}^{\infty} d\omega \left\{ |\, V_{ee}(q)\, |^2 - \frac{1}{2} V_{ee}(q)\, V_{ee}(\sqrt{4p^2 - q^2}) \right\} \Big/ |\, \varepsilon(q,\omega)\, |^2 \\ &\quad \times \delta\left[\omega - E_e(k) + E_e(k+q)\right] \delta\left[\omega + E_e(p) - E_e(p-q)\right] f_e(k)[1 - f_e(k+q)] \\ &\quad \times f_e(p)[1 - f_e(p-q)][K_n(k,q) + K_n(p,-q)][K_m(k,q) + K_m(p,-q)] ; \end{aligned} \tag{32}$$

$$\begin{aligned} D_{nm}^{ei} &= \pi\beta\hbar \sum_{k,p,q} \int_{-\infty}^{\infty} d\omega\, S_{ii}(q,\omega) \left| \frac{V_{ei}(q)}{\varepsilon(q,\omega)} \right|^2 \delta\left[\omega - E_e(k) + E_e(k+q)\right] \delta\left[\omega + E_i(p) - E_i(p-q)\right] f_e(k)[1 - f_e(k+q)] \\ &\quad \times f_i(p)[1 - f_i(p-q)]\, K_n(k,q) K_m(k+q,-q) . \end{aligned} \tag{33}$$

The electron-atom correlation function is treated within the second Born approximation in order to include besides the atomic form factor (first Born approximation $V^{(1)}$) also the polarization contributions (second Born approximation $V^{(2)}$). In the static case, we then have

$$\begin{aligned} D_{nm}^{ea} &= \pi\beta\hbar \sum_{k,nn'P,q} \left| V^{(1)}(knP, k+qn'P-q) + V^{(2)}(knP, k+qn'P-q) \right|^2 \\ &\quad \times \delta\left[E_e(k) + E_{nP} - E_e(k+q) - E_{n'P-q}\right] f_e(k)[1 - f_e(k+q)] \\ &\quad \times g_{nP}[1 + g_{n'P-q}]\, K_n(k,q) K_m(k+q,-q) . \end{aligned} \tag{34}$$

$g_{nP} = [\exp(\beta E_{nP} - \mu_e - \mu_i) - 1]^{-1}$ is the Bose distribution function for atoms in the internal state n with a total momentum P.

Restricting to the static limit $\omega \to 0$ also for the case of electron-electron and electron-ion scattering, the Born approximation for the collision terms can be improved systematically by considering the T matrix with respect to the Debye potential (11). For electron-atom scattering, we consider the T matrix with respect to an *effective* interaction potential, the sum of the first and second Born approximation in (34). Then, the correlation functions $D^{ec}_{nm}, c = i, a$ are expressed by transport cross sections Q^{ec}_T (for details, see [39,63]),

$$D^{ec}_{nm} = \frac{2\hbar}{3\pi^2} N_c \int_0^\infty dk k^3 [\beta E_e(k)]^{n+m} \times f_e(k)[1 - f_e(k)]\, Q^{ec}_T(k) \,. \tag{35}$$

For the nondegenerate case, Fermi distribution functions are replaced by Boltzmann factors. The electron-electron correlation function (32), valid for arbitrary degeneracy, can then be related to the transport cross section Q^{ee}_T according to

$$D^{ee}_{nm} = \frac{4}{3}\sqrt{\frac{2m}{\pi\beta}} n N_e \int_0^\infty dx x^3 R_{nm}(x) Q^{ee}_T(x) \exp(-x), \tag{36}$$

with $x = \beta\hbar^2 k^2/m$. The polynomials R_{nm} are given in [31,63].

In the low-density limit, the plasma is fully ionized (i.e., $D^{ea}_{nm} = 0$), and the momentum-dependent electron-electron and electron-ion transport cross sections $Q^{ee,ei}_T$ can be approximated by a generalized Coulomb logarithm $\ln\Lambda$ [63]. The transport coefficients are then given in the simple form

$$\begin{aligned} \sigma &= f \frac{(k_B T)^{3/2}(4\pi\varepsilon_0)^2}{e^2 m^{1/2}} \frac{1}{\ln\Lambda} \,, \\ \alpha &= a\, k_B/e \,, \\ \lambda &= L \left(\frac{k_B}{e}\right)^2 T\sigma \,. \end{aligned} \tag{37}$$

The convergence of this linear response method has been studied with respect to a systematic extension of the set of momenta $\{P_n\}$ [3,63,65]. In the nondegenerate limit, three momenta (P_0, P_1, P_2) are needed to reproduce the Spitzer results for the prefactors f, a, L in Eq. (37). Furthermore, there is a close connection to standard methods of kinetic theory for solving the Boltzmann equation. For instance, choosing Sonine polynomials for the set of relevant observables $\{P_n\}$ corresponds to the Chapman-Enskog method [66]. Considering Hermite polynomials coincides with the Grad method [67]. Solving the Boltzmann equation by means of a variational principle [68] or within the relaxation time approximation can also be related to special sets $\{P_n\}$ (for details, see [3,63,65]).

For the degenerate domain, Pauli blocking, structure factor, and local-field corrections to the dielectric function become of importance. The correlation functions can then be given in the Born approximation (Landau collision integral) by

$$\begin{aligned} D^{ec,L}_{nm} &= \frac{m^2\Omega_0^2\beta}{12\pi^3\hbar^3} \int_0^\infty dE\, (\beta E)^{n+m}\, U_{ec}(E) \\ &\quad \times f_e(E)[1 - f_e(E)] \,, \\ U_{ec}[E_e(k)] &= N_i \int_0^{2k} dq\, q^3 \left|\frac{V_{ec}(q)}{\varepsilon(q)}\right|^2 S_{ii}(q) \,. \end{aligned} \tag{38}$$

Already a one-momentum approximation (P_0) yields, e.g., the Ziman formula for the electrical conductivity, whereas the Mott formula for the thermopower and the Wiedemann-Franz relation for the thermal conductivity can be derived from a two-momentum approximation (P_0, P_1) and a three-momentum approximation (P_0, P_1, P_2), respectively.

C. Transport cross sections

The correlation functions D_{nm} are given in lowest density order by a ladder sum of diagrams, which corresponds to the Boltzmann collision term [31]. The respective T matrices relate the correlation functions to the two-particle scattering process, which is described by the transport cross sections $Q^{ec}_T(k)$ for elastic electron-electron, electron-ion, and electron-atom scattering ($c = e, i, a$),

$$Q^{ec}_T(k) = 2\pi \int_0^\pi \frac{d\sigma}{d\Omega} (1 - \cos^l\chi) \sin\chi\, d\chi \,. \tag{39}$$

The scattering angle χ is related to the transfer momentum by $q = 2k\sin(\chi/2)$, and $d\sigma/d\Omega$ is the differential scattering cross section. For ei and ea scattering we have $l = 1$, whereas for ee scattering $l = 2$ holds. Within a partial wave expansion for $Q^{ec}_T(k)$, the following expressions are derived:

$$Q^{ed}_T(k) = \frac{4\pi}{k^2} \sum_{\ell=0}^\infty (\ell+1) \sin^2\left[\delta^{ed}_\ell(k) - \delta^{ed}_{\ell+1}(k)\right] \,, \quad d = i, a \,, \tag{40}$$

$$Q^{ee}_T(k) = \frac{4\pi}{k^2} \sum_{\ell=0}^\infty \frac{(\ell+1)(\ell+2)}{2\ell+3} \left(1 - \frac{(-1)^\ell}{2}\right) \times \sin^2\left[\delta^{ee}_\ell(k) - \delta^{ee}_{\ell+2}(k)\right] \,.$$

The scattering phase shifts δ^{ec}_ℓ for electron-ion and electron-electron scattering have already been determined in Sec. II for the Debye potential (11) when calculating the two-particle partition functions Z_{ec}. The respective results for the transport cross sections (40) are shown in Fig. 3 as function of the screening length R_D. Figure 3(a) shows a very systematic behavior with respect to k, the transport cross sections are decreasing with density due to screening. The respective figures have been checked against earlier calculations [34,56].

For small R_D values ($R_D < 10a_B$), [see Fig. 3(b)], the electron-ion transport cross sections show resonancelike behavior for k values smaller than $0.8k_F$ due to the vanishing of the last bound states (e.g., $2s$ at $R_D = 3.223a_B$) in the energy spectrum and the consequences of the Levinson theorem. In this region, which is the main part of the integral interval, the transport cross sections vary by up to three orders of magnitude. For $k > k_F$, the transport cross sections are reduced with decreasing R_D values systematically.

As we will show in the next section, the ion-ion structure factor $S_{ii}(q)$ has to be taken into account at higher densities. Thus, the electron-ion transport cross section $Q_T^{ei}(k)$ derived from (39) has a more complicated form,

$$Q_T^{ei}(k) = \frac{\pi}{2k^2}\int_0^\pi \left|\sum_\ell (2\ell+1)\left[\exp(2i\delta_\ell^{ei})-1\right] P_\ell(\cos\chi)\right|^2 S_{ii}\left[2k\sin(\chi/2)\right](1-\cos\chi)\sin\chi\, d\chi\,, \tag{41}$$

where $P_\ell(x)$ are Legendre polynomials. We will discuss the respective results in Sec. IV.

For electron-atom scattering, the scattering phase shifts were also calculated numerically with respect to an appropriate potential; see (34). Utilizing the optical potential method for electron-neutral scattering, the second-order potential contains the atomic form factor (first Born approximation) as well as the polarization potential (second Born approximation). The respective results are displayed in Fig. 4.

The transport cross sections within the partial wave expansion (40) with respect to the polarization potential $V^{(2)} = V^{\mathrm{PP}}(R)$ (17) alone are compared for $R_D = (5, 20, \infty) \times a_B$ with those where the atomic form factor [69]

$$V^{(1)}(r) = -\frac{2e^2}{4\pi\varepsilon_0}\left(\frac{1}{a_B}+\frac{1}{r}\right)\exp(-2r/a_B)$$

has been included, i.e., $V^{(1)} + V^{(2)}$ as an effective potential. In addition, the ordinary Born approximation for the transport cross section with respect to the unscreened ($R_D = \infty$) polarization potential (dotted line), and the T

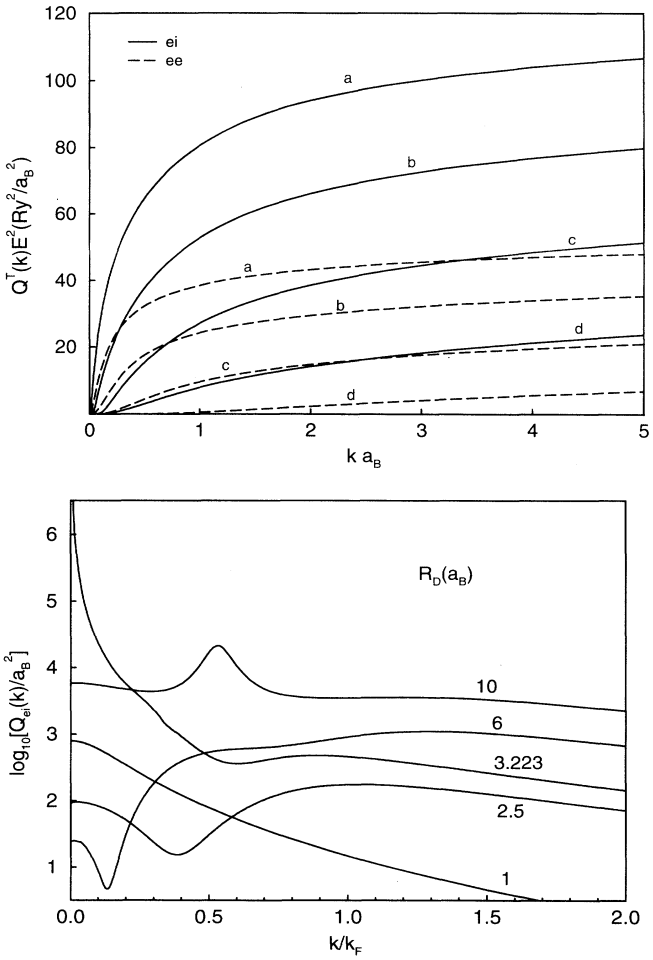

FIG. 3. (a) Transport cross sections for electron-ion (full curves) and electron-electron scattering (broken curves) as a function of the wave number vector $\mathbf{k}$ for various screening lengths R_D. a: $R_D = 10^3 a_B$; b: $R_D = 10^2 a_B$; c: $R_D = 10a_B$; d: $R_D = 1a_B$. (b) Transport cross sections for electron-ion scattering as a function of the normalized wave number vector k/k_F for various screening lengths R_D.

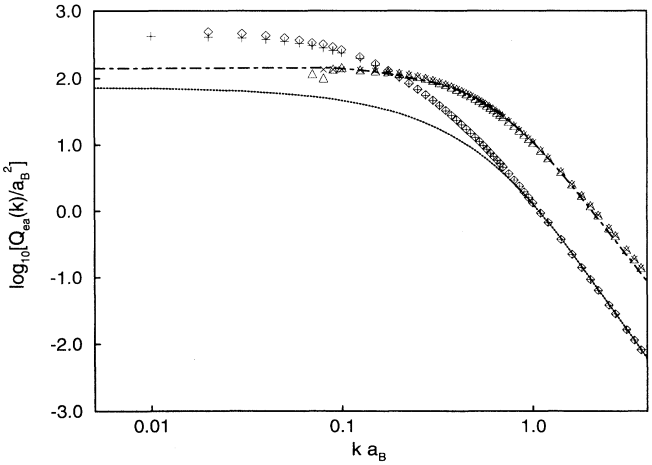

FIG. 4. Transport cross section for electron scattering at hydrogen atoms as a function of the wave number vector $\mathbf{k}$: utilizing only the polarization potential $V^{(2)}$ in Eq. (34) for the unscreened case ($\Diamond$) and $R_D = 20a_B$ (+); considering the atomic form factor in addition, i.e., $V^{(1)} + V^{(2)}$, for the unscreened case ($\times$) and $R_D = 20a_B$ ($\triangle$). For comparison, the ordinary Born approximation with respect to the unscreened polarization potential (dotted line) and the results of Meyer and Bartoli [70] within a T matrix calculation (dash-dotted line) are shown.

matrix results of Meyer and Bartoli [70] (dashed-dotted line) which obey the Friedel sum rule are shown.

In the Born approximation, the electron-atom transport cross section is considerably underestimated. The partial wave expansion with respect to the polarization potential alone gives results that are too high for low transfer momenta k. This has a pronounced influence on the transport coefficients in regions with a low degree of ionization, i.e., the partially ionized plasma region. A very good overall agreement with the consistent Meyer-Bartoli curve is found within the partial wave expansion with respect to the atomic form factor plus the polarization potential (see also [55] for alkali-atom plasmas). One can conclude that the atomic form factor is important for large transfer momenta k, and that there is no significant influence of screening on the electron-atom transport cross section. Therefore, the Meyer-Bartoli formula can be utilized for the further evaluation of the correlation functions D^{ea}_{nm}.

D. Ion-ion structure factor

For the calculation of force-force correlation functions (38) and, thus, also the transport coefficients L_{ik} (23), the ion-ion structure factor $S_{ii}(k)$ has to be determined. At low densities, i.e., for weakly coupled, nondegenerate plasmas, the system can be assumed to be randomly distributed with $S_{ii}(k) \approx 1$. At higher densities, both exchange and correlation contributions to the screening function lead to a typical oscillatory behavior of $S_{ii}(k)$.

In the fully ionized region, the plasma is usually described as a one-component system where the ions interact via an effective interaction potential $V^{\rm eff}_{ii}(r)$. The pure Coulomb potential $V_{ii}(r)$ is modified by the screening of the electrons, which can be described by the dielectric function $\varepsilon(k)$ according to Eq. (31). For $\varepsilon(k)$ we evaluate the full random phase approximation (RPA) numerically for arbitrary degeneracy of the electron system. To account for exchange and correlation effects, local-field corrections $G_e(k)$ are introduced by the relation

$$\Pi_e(k) = \frac{\Pi^{\rm RPA}_e(k)}{1 + V(k) G_e(k) \Pi^{\rm RPA}_e(k)} \,. \tag{42}$$

For $G_e(k)$, various expressions have been derived. We utilize here the parametrization given by Ichimaru and Utsumi [71], which satisfies the self-consistency conditions in the compressibility sum rule and the short-range correlation. The effective potential in coordinate space follows then from the Fourier transform of Eq. (31).

Figure 5 shows the drastic changes of the interionic potential with respect to a variation of the density (given by R_D) for a fixed temperature of $T = 10^4$ K. At high densities, the electron gas is fully degenerate and the strong screening leads to a short-range interionic potential. Local-field corrections are small in that region. At intermediate densities, the minimum of the interionic potential caused by the local-field corrections becomes more pronounced. At low densities, the minimum vanishes again and the behavior is Debye-like.

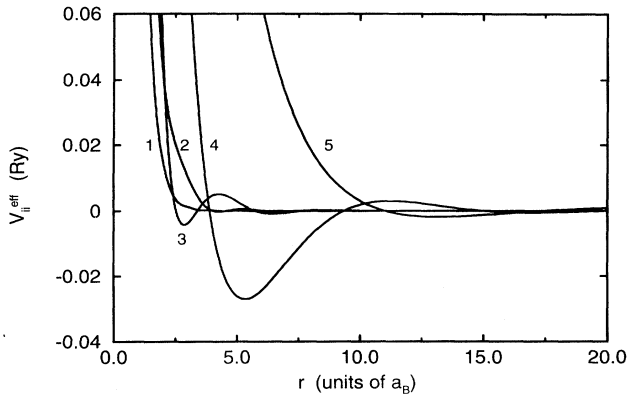

FIG. 5. Effective ion-ion potentials within full RPA including local-field corrections for $T = 10^4$ K and various R_D values. 1: $R_D = 0.5a_B$; 2: $R_D = 0.8a_B$; 3: $R_D = 1.0a_B$; 4: $R_D = 2.0a_B$; 5: $R_D = 5.0a_B$.

The ion-ion structure factor $S_{ii}(k)$ can be calculated numerically utilizing the integral equation method for the determination of the correlation functions. Within this scheme, the Ornstein-Zernike relation $h(\mathbf{r}) = c(\mathbf{r}) + n \int c(|\mathbf{r} - \mathbf{r}'|) h(\mathbf{r}')\, d\mathbf{r}'$ is supplemented by the closure relation

$$g_{ii}(r) = \exp\left(h(r) - c(r) - \frac{V^{\rm eff}_{ii}(r)}{k_B T} + B(r) \right) . \tag{43}$$

$c(r)$ is the direct correlation function, $h(r)$ the total correlation function with $h(r) = g(r) - 1$, and $g(r)$ the pair distribution function.

Neglecting the bridge function $B(r)$, the static structure factor

$$S_{ii}(q) = 1 + n \int d\mathbf{r}\, [g(r) - 1] \exp(i\mathbf{q} \cdot \mathbf{r}) \tag{44}$$

is calculated in the HNC approximation. For the numerical evaluation, we have employed the algorithm developed by Labik, Malijevski, and Vonka [72].

To check our calculation, the resulting structure factors at $\Gamma = 1$ and $\Theta = 0.1$ were compared with self-consistent results of Ichimaru and co-workers [51] for $S_{ii}(k)$ and $G_e(k)$ for a strongly coupled plasma, and a good agreement within 5% can be stated.

Figure 6 shows a typical sequence of structure factors for various densities according to the effective interionic potentials in Fig. 5. Due to the strong changes of the interionic potential, the qualitative behavior varies especially for small k values. For high densities ($R_D = 0.5a_B$), the compressibility of the system is low, and $S(k \to 0)$ is nearly zero. With decreasing density, up to $R_D = 2a_B$, the long-wavelength limit for the structure factor increases strongly. This behavior is mainly due to the attractive part of the potential, which becomes more pronounced in that region. With a further decrease of the density, this attractive part vanishes again and the structure factor drops down to values $S_{ii}(k \to 0) < 1$.

We want to state that the small k behavior of the

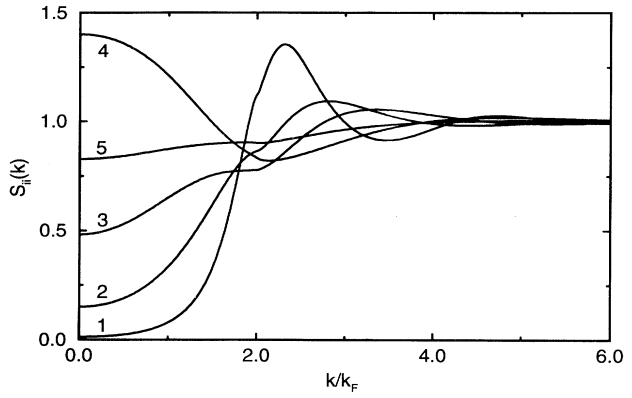

FIG. 6. Ion-ion structure factor within full RPA including local-field corrections for $T = 10^4$ K and various R_D values (see Fig. 5). 1: $R_D = 0.5a_B$; 2: $R_D = 0.8a_B$; 3: $R_D = 1.0a_B$; 4: $R_D = 2.0a_B$; 5: $R_D = 5.0a_B$.

structure factor as derived from the HNC approximation corresponds to the compressibility of an electron gas treated in extended RPA. The present equation of state, however, contains also contributions of bound states, of a hard core reference system, etc. (see Sec. II). Therefore, the present structure factors that are needed for the calculation of the transport coefficients in the high density region are not internally consistent with this equation of state.

IV. RESULTS FOR THE TRANSPORT COEFFICIENTS

The electrical conductivity σ, thermal conductivity λ, and thermopower α of partially ionized hydrogen plasma were calculated for $T = 10^4 - 10^5$ K and $n_e = 10^{16} - 10^{25}$ cm^{-3}.

In the high density limit, the consideration of higher momenta $\mathbf{P}_n$ corresponds to a generalization of the Ziman (and Mott) formula as employed, e.g., in [50,51]. We have included structure factor effects as well as local-field corrections when calculating the correlation functions D^{ei}_{nm} in that region. Taking into account the structure factor for electron-ion scattering via (41), we found only little impact on the transport properties. Especially for high temperatures structure factor effects can be neglected. For $T \leq 10^4$ K and $R_D > 1a_B$, the transport cross section is reduced by only 1%. On the contrary, for $R_D \leq 1a_B$, we find a pronounced lowering of the transport cross sections especially for small $\mathbf{k}$ values so that these contributions are damped out when integrating over $\mathbf{k}$. This leads to a lowering of the electron-ion correlation function by up to one order of magnitude in the high-density–low-temperature domain, which is considered to represent a metallic liquid.

Furthermore, the composition of hydrogen plasma was determined considering the nonideality corrections to the thermodynamic potentials and the respective laws of mass action; see Sec. II. Thus, also the region of partial ionization at intermediate densities and low temperatures has been covered.

The numerical results obtained within the present linear response approach interpolate between the Spitzer theory for nondegenerate, weakly nonideal plasmas [see (37)] and the Ziman theory for degenerate, strongly coupled plasmas. This is demonstrated in Figs. 7–9 where the transport coefficients are shown for a given temperature of $T = 15 \times 10^3$ K as function of the number density. A three-momentum approximation has been applied, i.e., utilizing $\mathbf{P}_0, \mathbf{P}_1$, and $\mathbf{P}_2$, which yields an accuracy of 1% compared with the values obtained within an infinite series expansion of the distribution function.

The correlation functions were calculated on the T matrix level using (40) for electron-electron scattering, (41) for electron-proton scattering, and, for simplicity, the fit formula of Meyer and Bartoli [70] for electron-atom scattering; see Fig. 4. The scattering of electrons at dimers was supposed to follow a potential strength similar to that of atoms so that the interaction of electrons with *all* neutrals is described by this formula.

The results for the electrical conductivity and thermopower indicated with *generalized Ziman* and *Mott formula* have been deduced from the first Born approximation for the electron-ion correlation function (38) within a one- and two-momentum approximation, respectively. Electron-electron and electron-neutral interactions have been neglected in this Lorentz plasma model. However, the effects of structure factor and of a smeared-out Fermi surface (arbitrary degeneracy) are included.

A. Electrical conductivity

The electrical conductivity (Fig. 7) is given by the Spitzer formula in the low-density limit up to 10^{18} cm^{-3}

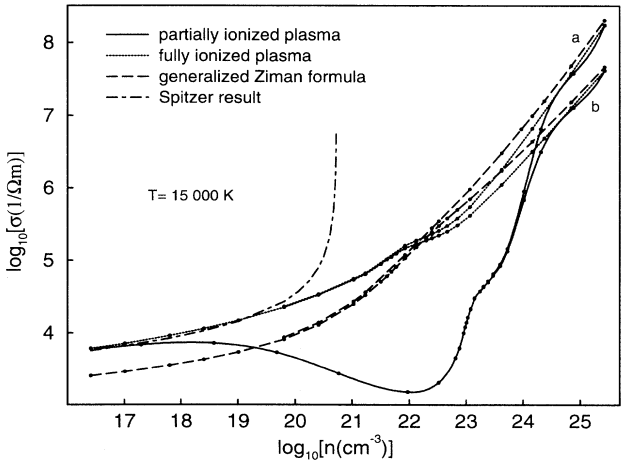

FIG. 7. Electrical conductivity σ of hydrogen plasma for $T = 15 \times 10^3$ K as a function of the particle number density n within different models: Spitzer curve [47] (dash-dotted line), generalized Ziman formula (dashed line), fully ionized plasma within the T matrix approximation (dotted line), partially ionized plasma within the T matrix approximation (full line) including (a) and neglecting (b) the structure factor.

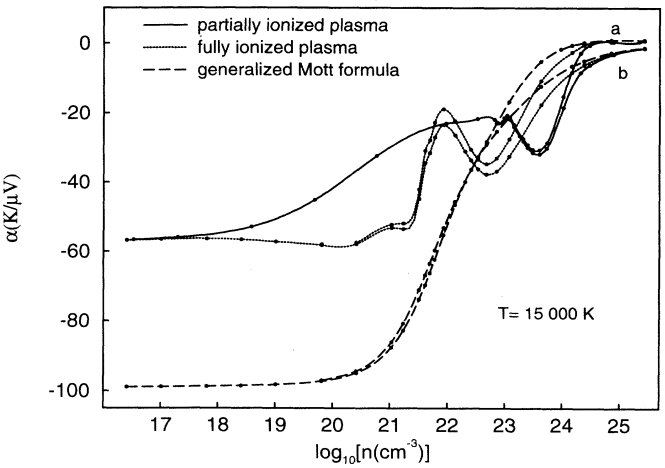

FIG. 8. Thermopower α of hydrogen plasma for $T = 15 \times 10^3$ K as a function of the particle number density n within different models: generalized Mott formula for the Lorentz plasma (only electron-ion interaction, dashed line), fully ionized plasma within the T matrix approximation (dotted line), partially ionized plasma within the T matrix approximation (full line) including (a) and neglecting (b) the structure factor.

and has typical values of $\sigma \approx 10^4/(\Omega\ \mathrm{m})$. The Spitzer curve diverges for higher densities. The T matrix results for the fully ionized plasma merge into the Ziman formula above 10^{22} cm^{-3}. This is a result of the strong screening of the Coulomb interaction so that the first Born approximation becomes valid. Furthermore, the electron distribution function is determined already by one momentum $\mathbf{P}_0$ in the degenerate domain, whereas two three momenta $\mathbf{P}_n$ are needed in the nondegenerate region. Employing the Ziman formula also for nondegenerate plasmas leads to conductivities that are too low by a factor of about two.

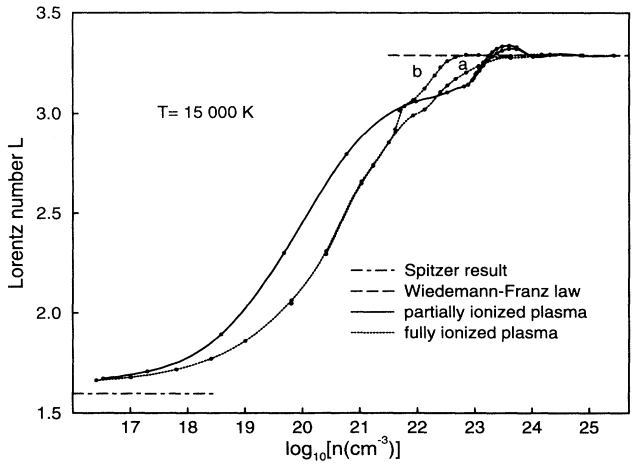

FIG. 9. Lorentz number L of hydrogen plasma for $T = 15 \times 10^3$ K as a function of the particle number density n within different models: Spitzer result [47] (dash-dotted line), Wiedemann-Franz law (dashed line), fully ionized plasma within the T matrix approximation (dotted line) including (a) and neglecting (b) the structure factor, partially ionized plasma within the T matrix approximation (full line).

Partial ionization of the plasma, i.e., the formation of neutral and charged clusters, leads to a strong decrease and a typical minimum behavior of the isotherms for the electrical conductivity. The decrease is a result of the diminishing fraction of free electrons and their reduced mobility due to scattering at neutrals. The minima occur at about 10^{22} cm^{-3} and run to values less than $\sigma \approx 10^2/(\Omega\ \mathrm{m})$ dependent on temperature (see Fig. 10). The conductivity shows then a subsequent sharp increase due to the Mott effect, i.e., the bound states vanish, and the plasma becomes fully ionized again. Furthermore, electron-electron and electron-neutral scattering is no longer of importance so that the free electron mobility is also increasing. Ion-ion correlations are described by the structure factor in the electron-ion correlation function (41) and lead to a sharper increase of the conductivity in the high-density (liquid) branch compared with the case of $S(k) = 1$.

This typical behavior at low temperatures can be interpreted as a nonmetal-to-metal transition. Utilizing the Mott criterion for the minimum metallic conductivity of $\sigma \approx 10^4/(\Omega\ \mathrm{m})$ also for $T \neq 0$ in order to locate this transition, a critical density of about 0.16 g cm^{-3} can be found that is close to the critical density of the thermodynamic instability at 0.42 g cm^{-3}; see Sec. II.

B. Thermopower

The general behavior of the thermopower is shown in Fig. 8. Again, the low-density asymptote within the present T matrix approximation for the fully ionized plasma coincides with the Spitzer result, $\alpha = -60.60$ μV K^{-1}. The high-density limit is given by the Mott formula. However, already the T matrix results for the fully ionized case show an interesting behavior between 10^{21} cm^{-3} and the critical density of 10^{23} cm^{-3}. In this region, a resonancelike behavior of the scattering phase shift sum that enters into the expression for the electron-ion transport cross section (40) is obtained when the lowest bound states $(1s, 2s, 2p, \ldots)$ disappear (see Sec. III C). For the thermopower, two Onsager coefficients L_{ik} have to be determined according to Eq. (22) which average this resonancelike behavior in different ways so that we obtain a "wiggle" for the thermopower. This distinct behavior of the thermopower has already been found for hydrogenlike systems such as cesium plasma [73]. Furthermore, the density region between the local maximum and the local minimum of the thermopower is connected with the decreasing slope of the curve for the electrical conductivity in Fig. 7.

The Mott formula (Born approximation) yields values for the thermopower that are too small by a factor of about two in the low-density limit. In addition, the influence of electron-electron scattering that is important in that region is not accounted for in this Lorentz plasma model.

Consideration of partial ionization leads to drastic ef-

fects. At about 10^{18} cm^{-3}, a strong increase up to slightly negative values is found. However, positive values for the thermopower as proposed earlier in that domain [3] could not be verified. This might be an inherent feature of the Born approximation for the collision integrals D_{nm} and/or result from the simpler evaluation of the equation of state within the Debye-Hückel approximation utilized in that paper.

Taking into account ion-ion correlations again, the sharp increase of the thermopower becomes more pronounced in the high-density–low-temperature region, i.e., for $T \leq 15 \times 10^3$ K and $n \geq 10^{24}$ cm^{-3}. Furthermore, small positive values and, thus, a change of sign have been obtained. A similar behavior was recently found for liquid Cs [74] as a result of structure factor effects and local-field corrections.

It would be of high interest to calculate the thermopower along the liquid-vapor coexistence curve of mercury within our improved model where such strong positive values for the thermopower have been measured [75]. Then, general conditions for the coincidence of the density for the zero-point transition of the thermopower and the critical density of the liquid-vapor phase transition as found for mercury can be verified.

C. Lorentz number

The thermal conductivity behaves very similar to the electrical conductivity so that we have plotted in Fig. 9 the Lorentz number

$$L = \frac{e^2}{k_B^2 T} \frac{\lambda}{\sigma} . \tag{45}$$

For the nondegenerate case, the Lorentz number is 4.0 for a Lorentz plasma (only electron-ion interaction), or 1.5966 considering also electron-electron scattering. For the degenerate domain, the Wiedemann-Franz relation is fulfilled, which gives $L = \pi^2/3$. In the intermediate region, the numerical results for (45) interpolate between these limiting cases dependent on temperature. Again, the oscillatory behavior at densities between 10^{23} and 10^{24} cm^{-3} stems from the resonancelike structures in the scattering phase shift sum as already discussed for the thermopower. Ion-ion correlations have little influence on the Lorentz number in the partially ionized domain and yield only a small reduction of the values.

D. Metal-nonmetal transition and comparison

In Figs. 10–12, the present results for the transport coefficients are shown for various temperatures as a function of the number density. The deep minima for the electrical (Fig. 10) and thermal conductivity (Fig. 12) vanish above $T = 30 \times 10^3$ K because the plasma remains nearly fully ionized over the entire density domain. For low temperatures, a steep increase of the conductivities over four orders of magnitude in the narrow density region around 10^{23} cm^{-3} can be seen, which clearly

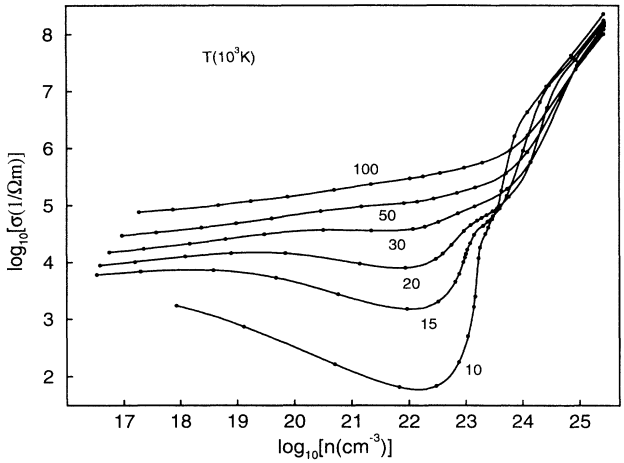

FIG. 10. Electrical conductivity σ for partially ionized hydrogen plasma for various temperatures as a function of the particle number density n.

demonstrates the occurrence of a smooth nonmetal-to-metal transition near the critical point of the hypothetical plasma phase transition.

Another indication for such a transition is the strong increase of the thermopower towards positive values and the subsequent steep slope in that density region (Fig. 11). This behavior is similar to that observed experimentally for mercury along the coexistence line [75], although high positive values for the thermopower could not be verified for hydrogen plasma at the nonmetal-to-metal transition contrary to the mercury results.

There are few experimental data for the transport coefficients of dense hydrogen plasma [76] but some other theoretical approaches exist. For instance, Boercker, Rogers, and DeWitt [50] determined the electrical conductivity for strongly coupled plasmas within the Chapman-Enskog scheme for solving the Gould-DeWitt kinetic equation [54]. They calculated the correct quantum, De-

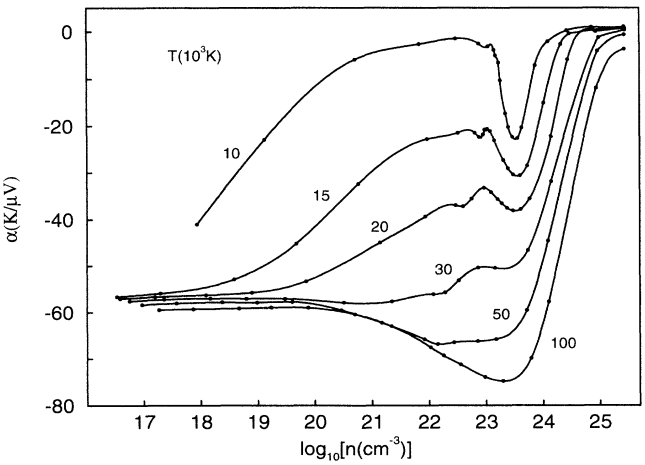

FIG. 11. Thermopower α for partially ionized hydrogen plasma for various temperatures as function of the particle number density n.

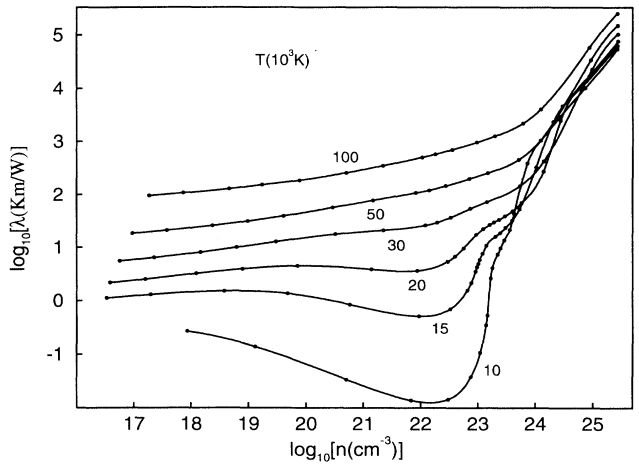

FIG. 12. Thermal conductivity λ for partially ionized hydrogen plasma for various temperatures as function of the particle number density n.

bye screened cross sections for electrons scattering from finite-sized ions, neutrals, and other electrons. Their scheme coincides completely with the present approach in the nondegenerate case.

The correlation function method utilized by Ichimaru and Tanaka [51] is based on the Ziman formula for $Z = 1$ and yields conductivities between the T matrix results and the generalized Ziman formula. A prefactor was adopted to give the right Spitzer values in the low-density limit. In the high-density limit, structure factor effects and local-field corrections have been included self-consistently, which goes beyond the present approach.

Djurić *et al.* [77] derived a fit formula for the electrical conductivity based on the Ziman formula for $Z = 1$ taking into account screened Coulomb interactions and local-field corrections and obtained slightly smaller results than those of Ichimaru and Tanaka.

Rinker [52] also utilized the Ziman formula to calculate the electrical and thermal conductivity for a large domain of the density-temperature plane, whereas the conductivity model of Lee and More [60] is based on the relaxation time approximation, which neglects electron-electron correlations. Both models are valid for $Z \geq 1$ and arbitrary degeneracy.

V. CONCLUSIONS

We have presented a quantum-statistical approach to the equation of state and the transport properties of dense hydrogen plasma. A thermodynamic instability has been found within the chemical picture where the critical point coincides with results of Ebeling and Richert [8,9], and Saumon and Chabrier [6,7] for the hypothetical plasma phase transition. Within our approach, at least the two-particle correlations have been accounted for correctly by an improved Beth-Uhlenbeck formula. The concentration of higher clusters such as dimers H_2 and molecular ions H_2^+ has been determined from respective laws of mass action. Near the instability region, all species have strongly varying concentrations, which indicates the significant influence of nonideality corrections on the thermodynamic functions.

The implications of this thermodynamic stability behavior on the transport properties have been studied for weakly coupled, nondegenerate plasmas up to strongly coupled, degenerate plasmas. We have utilized a generalized linear response approach in the formulation of Zubarev [20], which yields the Spitzer as well as the Ziman theory as limiting cases.

Again, two-particle correlations have been accounted for by the correct quantum cross sections for electron scattering at ions and free electrons. Electron scattering at neutral atoms was also considered on a T matrix level with respect to an effective optical potential. Strong ion-ion correlations are of special importance at high densities. The respective ion-ion structure factor was determined numerically within the HNC scheme, taking into account local-field corrections to the screening function of the effective ion-ion interaction potential.

The results for the transport coefficients clearly indicate that a nonmetal-to-metal transition occurs near the critical point of the hypothetical plasma phase transition. This can be seen from the sharp but smooth increase of the conductivities and from the drastic shift of the thermopower towards positive values in a narrow density range. This typical behavior is a consequence of the vanishing of neutral two-particle states (atoms) with increasing density, which is usually described as a *Mott transition.* Subsequently, the fraction of free conduction electrons that is determined by the ionization degree increases strongly. Although the energy levels of the atom disappear one after another, this transition is a continuous one because the respective contributions are taken over by the scattering states. This is a general characteristic of the physical picture which treats bound and scattering states on the same level. This concept was applied in this paper at least for two-particle correlations when calculating the two-particle partition function Z_e, Eq. (9).

Such a continuous behavior has already been found by Höhne and Zimmermann [78] for the oscillator strength of hydrogen atoms as a function of the density. As a consequence, a *transparency window* in dense plasmas as predicted by some authors [79] for the region where only one bound state remains is very unlikely to occur. Nevertheless, due to the Levinson theorem, a resonancelike behavior is obtained in the electron-ion scattering cross section whenever a bound state disappears. In particular, the vanishing of the lowest-energy levels in hydrogen yields the distinctive structures that are apparent in the conductivities and the thermopower; see Figs. 7–9.

The nonmetal-to-metal transition discussed for hydrogen is experimentally verified for expanded alkali-atom metals and mercury from measurements of the thermoelectric, structure, magnetic, and optical properties [23,24]. There, the transition occurs near the critical point of the liquid-vapor phase transition so that the thermodynamic properties of the system have to be determined considering simultaneously the drastic varia-

tion of the electronic properties. Quantum-statistical approaches have been successful in describing general features of such a combined thermodynamic and electronic transition for the alkali-atom metals [25,30,36,80] and mercury [36,81]. Therefore, the present approach *supports* the presence of a thermodynamic instability in dense hydrogen plasma—the hypothetical plasma phase transition—with a second critical point at about $T_c = 16 \times 10^3$ K and $p_c = 60$ GPa, far apart from that of the ordinary liquid-vapor phase transition.

However, the present approach is also based on the chemical picture when treating higher clusters such as H_2 or H_2^+ and the various interactions between the species. Therefore, we are not able to decide whether or not this plasma phase transition is a *real* thermodynamic phase transition with a second critical point, or an artefact of that approach. The occurrence of the nonmetal-to-metal transition is *not* affected by that shortcoming of the theory so that it can serve as a precursor for a real phase transition.

A more detailed theoretical approach should be based on a consistent physical picture. Simultaneously, one should go beyond the quasiparticle picture by taking into account the damping of one- and two-particle states via the imaginary parts of the self-energy. For this, the spectral function in Eq. (9) has to be determined self-consistently for a Coulomb system at arbitrary degeneracy. Having in mind the relatively simple approximations that were utilized for the evaluation of the expressions for some of the nonideality corrections, this problem seems to have been out of reach until now. Furthermore, typical effects for solid-state-like densities such as band structure and disorder should be taken into account in a more unified approach.

The estimate for the discontinuity of the density between the two hypothetical phases is 20% according to Saumon and Chabrier [7]. A direct observation of this discontinuity might be difficult in strongly coupled plasmas. Therefore, it should be of great interest to study the behavior of other quantities that are directly correlated with the equation of state data as, for instance, the transport properties. Further quantities to be discussed are, for instance, stopping power, opacity, or reflectivity in order to narrow down the parameter domain where future experiments have to look for precursors of the (up to now) hypothetical plasma phase transition.

Besides hydrogen, other systems are also candidates for the observation of a plasma phase transition. Inert gases are especially well suited for that purpose because clusters do not occur virtually and the polarizability of neutrals is small, which implies weak polarization and van der Waals interaction. Therefore, inert gas plasmas can be treated theoretically within the *physical picture* adequately contrary to hydrogen plasma. The effective, but limited concept of a *chemical picture* has already been applied to inert gas plasmas [15], and yields results very similar to those for hydrogen plasma. Advanced shock-wave techniques have been applied, e.g., to xenon [16], which are considered to be eligible of reaching the proposed instability region so that the phase transition could be studied experimentally. Furthermore, new techniques such as ultrashort, high-intensity laser beams [82] or high-energy heavy ion beams [83] should be utilized to produce strongly coupled plasmas with parameters in the required range.

ACKNOWLEDGMENTS

Discussions with G. Röpke, D. Kremp, W.D. Kraeft, M. Schlanges, J. Meyer-ter-Vehn, Y.W. Kim, and A. Förster are gratefully acknowledged. This research was supported by the Deutsche Forschungsgemeinschaft within the SFB 198 "Kinetics of Partially Ionized Plasmas."

[1] S. Ichimaru, Rev. Mod. Phys. **54**, 1015 (1982). For a review of plasma parameters see also S. Ichimaru, *Plasma Physics* (Benjamin, Menlo Park, CA, 1986).

[2] W.-D. Kraeft, D. Kremp, W. Ebeling, and G. Röpke, *Quantum Statistics of Charged Particle Systems* (Plenum, New York, 1986).

[3] F.E. Höhne, R. Redmer, G. Röpke, and H. Wegener, Physica (Amsterdam) **128A**, 643 (1984).

[4] H.K. Mao and R.J. Hemley, Rev. Mod. Phys. **66**, 671 (1994).

[5] W.J. Nellis, A.C. Mitchell, P.C. McCandless, D.J. Erskine, and S.T. Weir, Phys. Rev. Lett. **68**, 2937 (1992).

[6] D. Saumon and G. Chabrier, Phys. Rev. A **44**, 5122 (1991); Phys. Rev. Lett. **62**, 2397 (1989).

[7] D. Saumon and G. Chabrier, Phys. Rev. A **46**, 2084 (1992).

[8] W. Ebeling and W. Richert, Ann. Phys. (Leipzig) **39**, 362 (1982).

[9] W. Ebeling and W. Richert, Phys. Status Solidi B **128**, 467 (1985); Phys. Lett. A **108**, 80 (1985); Contrib. Plasma Phys. **25**, 1 (1985).

[10] M. Robnik and W. Kundt, Astron. Astrophys. **120**, 227 (1983).

[11] P. Haronska, D. Kremp, and M. Schlanges, Wiss. Z. Univ. Rostock **36**, 98 (1987).

[12] D. Kremp, W.D. Kraeft, and M. Schlanges, Contrib. Plasma Phys. **33**, 567 (1993); M. Schlanges, M. Bonitz, and A. Tschttschjan, *ibid.* **35**, 109 (1995).

[13] A. Förster, T. Kahlbaum, and W. Ebeling, Laser Part. Beams **10**, 253 (1992).

[14] W. Ebeling, in *Inside the Sun*, edited by G. Berthomieu and M. Cribier (Kluwer Academic, Dordrecht, 1990), p. 43.

[15] W. Ebeling, A. Förster, W. Richert, and H. Hess, Physica (Amsterdam) **150A**, 159 (1988).

[16] W.J. Nellis, A.C. Mitchell, M. Van Thiel, G.J. Devine, and R.J. Trainor, J. Chem. Phys. **79**, 1480 (1983).

[17] L.P. Kadanoff and G. Baym, *Quantum Statistical Mechanics* (Wiley, New York, 1962).

[18] R. Zimmermann and H. Stolz, Phys. Status Solidi B **131**, 151 (1985).

[19] G.E. Beth and E. Uhlenbeck, Physica **3**, 729 (1936); **4**,

915 (1937).
[20] D.N. Zubarev, *Nonequilibrium Statistical Thermodynamics* (Consultants Bureau, New York, 1974).
[21] G. Röpke, Physica (Amsterdam) **121A**, 92 (1983).
[22] G. Röpke, Phys. Rev. A **38**, 3001 (1988).
[23] F. Hensel and H. Uchtmann, Ann. Rev. Phys. Chem. **40**, 61 (1989).
[24] F. Hensel, J. Phys.: Condens. Matter **2**, SA33 (1990).
[25] R. Redmer and G. Röpke, Contrib. Plasma Phys. **29**, 343 (1989).
[26] R. Redmer and G. Röpke, Physica (Amsterdam) **130A**, 523 (1985).
[27] R. Redmer, T. Rother, K. Schmidt, W.D. Kraeft, and G. Röpke, Contrib. Plasma Phys. **28**, 41 (1988).
[28] D. Bollé, Ann. Phys. (N.Y.) **121**, 131 (1979); see also his contribution in *Strongly Coupled Plasma Physics*, edited by F.J. Rogers and H.E. DeWitt (Plenum, New York, 1987), p. 215.
[29] F.J. Rogers, Astrophys. J. **310**, 723 (1986); see also his contribution in *Strongly Coupled Plasma Physics* (Ref. [28]), p. 261.
[30] R. Redmer and W.W. Warren, Jr., Phys. Rev. B **48**, 14 892 (1993); Contrib. Plasma Phys. **33**, 374 (1993).
[31] R. Redmer, G. Röpke, F. Morales, and K. Kilimann, Phys. Fluids B **2**, 390 (1990).
[32] F.J. Rogers, Phys. Rev. A **4**, 1145 (1971); see also F.J. Rogers, H.C. Graboske, Jr., and D.J. Harwood, Phys. Rev. A **1**, 1577 (1970).
[33] R. Zimmermann, *Many-Particle Theory of Highly Excited Semiconductors* (Teubner, Leipzig, 1988), p. 117.
[34] F. Sigeneger, S. Arndt, R. Redmer, M. Luft, D. Tamme, W.-D. Kraeft, G. Röpke, and T. Meyer, Physica (Amsterdam) **152A**, 365 (1988).
[35] V.A. Alekseev and I.T. Iakubov, Phys. Rep. **96**, 1 (1983). Cluster models have been applied for the calculation of the electrical conductivity of partially ionized alkali-metal plasmas by V.V. Gogoleva, V.Yu. Zitserman, A.Ya. Polishchuk, and I.T. Iakubov, Teplofiz. Vys. Temp. **22**, 208 (1984).
[36] J.P. Hernandez, Phys. Rev. Lett. **53**, 2320 (1984); Phys. Rev. A **31**, 932 (1985); Phys. Rev. Lett. **57**, 3183 (1986); Phys. Rev. A **34**, 1316 (1986).
[37] M. Gell-Mann and K.A. Brueckner, Phys. Rev. **106**, 364 (1957).
[38] W. Ebeling and H. Lehmann, Ann. Phys. (Leipzig) **45**, 529 (1988); see also S. Tanaka, S. Mitake, X.-Z. Yan, and S. Ichimaru, Phys. Rev. A **32**, 1779 (1985).
[39] R. Redmer, G. Röpke, and R. Zimmermann, J. Phys. B **20**, 4069 (1987).
[40] J.A. Barker and D. Henderson, J. Chem. Phys. **47**, 2856 (1967); **47**, 4714 (1967); Rev. Mod. Phys. **48**, 587 (1976).
[41] J. Aviram, S. Goshen, and R. Thieberger, J. Chem. Phys. **62**, 425 (1975); J. Aviram, Y. Rosenfeld, and R. Thieberger, J. Chem. Phys. **64**, 4741 (1976).
[42] G.A. Mansoori, N.F. Carnahan, K.E. Starling, and T.W. Leland, J. Chem. Phys. **54**, 1523 (1971); see also W. Ebeling and K. Scherwinski, Z. Phys. Chem. (Leipzig) **264**, 1 (1983).
[43] T.H. Miller and B. Bederson, Adv. At. Mol. Phys. **13**, 1 (1977).
[44] D.G. Hummer and D. Mihalas, Astrophys. J. **331**, 794 (1988); D. Mihalas, W. Däppen, and D.G. Hummer, *ibid.* **331**, 815 (1988).
[45] B. Bernu and J. Wallenborn, Europhys. Lett. **14**, 203 (1991).
[46] H. Hess and W. Ebeling, in *Strongly Coupled Plasma Physics* (Ref. [28]), p. 185; see also H. Hess, High Pressure Res. **1**, 203 (1989).
[47] L. Spitzer, Jr. and R. Härm, Phys. Rev. **89**, 977 (1953); L. Spitzer, Jr., *The Physics of Fully Ionized Gases* (Interscience, New York, 1960).
[48] J.M. Ziman, Philos. Mag. **6**, 1013 (1961).
[49] M. Baus, J.-P. Hansen, and L. Sjögren, Phys. Lett. A **82**, 180 (1981); H. Minoo, C. Deutsch, and J.-P. Hansen, Phys. Rev. A **14**, 840 (1976).
[50] D.B. Boercker, F.J. Rogers, and H.E. DeWitt, Phys. Rev. A **25**, 1623 (1982). See also D.B. Boercker, *ibid.* **23**, 1969 (1981); F.J. Rogers, H.E. DeWitt, and D.B. Boercker, Phys. Lett. A **82**, 331 (1981).
[51] S. Ichimaru and S. Tanaka, Phys. Rev. A **32**, 1790 (1985); see also S. Ichimaru, H. Iyetomi, and S. Tanaka, Phys. Rep. **149**, 91 (1987); S. Tanaka, X.-Z. Yan, and S. Ichimaru, Phys. Rev. A **41**, 5616 (1990).
[52] G. Rinker, Phys. Rev. B **31**, 4207 (1985); **31**, 4220 (1985); Phys. Rev. A **37**, 1284 (1988).
[53] F.J. Rogers, H.E. DeWitt, and D.B. Boercker, Phys. Lett. A **82**, 331 (1981).
[54] H. Gould and H.E. DeWitt, Phys. Rev. **155**, 68 (1967); see also R.H. Williams and H.E. DeWitt, Phys. Fluids **12**, 2326 (1969).
[55] F. Bialas, K. Schmidt, M. Schlanges, and R. Redmer, Contrib. Plasma Phys. **29**, 413 (1989).
[56] S. Arndt, F. Sigeneger, F. Bialas, W.D. Kraeft, M. Luft, T. Meyer, R. Redmer, G. Röpke, and M. Schlanges, Contrib. Plasma Phys. **30**, 273 (1990).
[57] Yu.K. Kurilenkov and A.A. Valuev, Contrib. Plasma Phys. **24**, 529 (1984).
[58] R.J. Zollweg and R.W. Liebermann, J. Appl. Phys. **62**, 3621 (1987).
[59] R.B. Mohanti and J.G. Gilligan, J. Appl. Phys. **68**, 5044 (1990).
[60] Y.T. Lee and R.M. More, Phys. Fluids **27**, 1273 (1984).
[61] V. Christoph and G. Röpke, Phys. Status Solidi B **131**, 11 (1985).
[62] For the usual relations of irreversible thermodynamics see, for instance, S.R. DeGroot and P. Mazur, *Nonequilibrium Thermodynamics* (North-Holland, Amsterdam, 1962).
[63] H. Reinholz, R. Redmer, and D. Tamme, Contrib. Plasma Phys. **29**, 395 (1989).
[64] G. Röpke and R. Der, Phys. Status Solidi B **92**, 501 (1979). For a more detailed discussion, see Chap. 4.5. of Ref. 2.
[65] G. Röpke and F.E. Höhne, Phys. Status Solidi B **107**, 603 (1981).
[66] S. Chapman and T.G. Cowling, *The Mathematical Theory of Non-uniform Gases* (University Press, Cambridge, 1958).
[67] H. Grad, in *Handbuch der Physik, Vol. XXII*, edited by S. Flügge (Springer, Berlin, 1958), p. 205.
[68] J. Appel, Phys. Rev. **122**, 1760 (1961). For the variational principle, see M. Kohler, Z. Phys. **124**, 772 (1948); **125**, 679 (1949).
[69] N.F. Mott and H.S.W. Massey, *The Theory of Atom Collisions* (Oxford Univer. Press, New York, 1965).
[70] J.R. Meyer and F.J. Bartoli, Phys. Rev. B **24**, 2089 (1981).
[71] S. Ichimaru and K. Utsumi, Phys. Rev. B **24**, 7385

(1981); see also K. Utsumi and S. Ichimaru, *ibid.* **22**, 1522 (1980); **22**, 5203 (1980).

[72] S. Labik, A. Malijevsky, and P. Vonka, Mol. Phys. **56**, 709 (1985).

[73] V.A. Alekseev, A.A. Vedenov, V.G. Ovcharenko, L.S. Krasitskaya, Yu.F. Rhyzhkov, and A.N. Starostin, High Temp.-High Press. **7**, 677 (1975).

[74] H. Reinholz and R. Redmer, J. Non-Cryst. Solids **156-158**, 654 (1993).

[75] W. Götzlaff, G. Schönherr, and F. Hensel, Z. Phys. Chem. N.F. **156**, 219 (1988); see also W. Götzlaff, Ph.D. thesis, Philipps-Universität Marburg, 1988.

[76] Experimental and theoretical data for the electrical conductivity are reviewed, e.g., in K. Günther and R. Radtke, *Electric Properties of Weakly Nonideal Plasmas* (Akademie-Verlag, Berlin, 1984); W. Ebeling, V.E. Fortov, Yu.L. Klimontovich, N.P. Kovalenkov, W.D. Kraeft, Yu.P. Krasny, D. Kremp, P.P. Kulik, V.A. Riabii, G. Röpke, E.K. Rozanov, and M. Schlanges, *Transport Properties of Dense Plasmas* (Birkhäuser, Basel, 1984); V.E. Fortov and I.T. Iakubov, *Physics of Nonideal Plasmas* (Hemisphere Publishers, New York, 1990); and by I.T. Iakubov, Usp. Fiz. Nauk, **163**, 35 (1993).

[77] Z. Djurić, A.A. Mihajlov, V.A. Nastasyuk, M.M. Popović, and I.M. Tkachenko, Phys. Lett. A **155**, 415 (1991).

[78] F.E. Höhne and R. Zimmermann, J. Phys. B **15**, 2551 (1982).

[79] G.A. Kobzev, Yu.K. Kurilenkov, and G.E. Norman, Teplofiz. Vys. Temp. **15**, 193 (1977); G.A. Kobzev and Yu.K. Kurilenkov, *ibid.* **16**, 458 (1978); S.P. Vetsinin and Yu.K. Kurilenkov, *ibid.* **18**, 225 (1980).

[80] R. Redmer, H. Reinholz, G. Röpke, R. Winter, F. Noll, and F. Hensel, J. Phys. Condens. Matter **4**, 1659 (1992).

[81] G. Röpke, S. Nagel, and R. Redmer, Contrib. Plasma Phys. **33**, 0441 (1993); S. Nagel, G. Röpke, R. Redmer, and F. Hensel, J. Phys. Condens. Matter **6**, 2137 (1994).

[82] Th. Löwer *et al.*, Phys. Rev. Lett. **72**, 3186 (1994); J. Meyer-ter-Vehn, A. Oparin, and T. Aoki, in Proceedings of the 12th International Conference on Laser Interaction and Related Plasma Phenomena, Osaka, 1995 (unpublished).

[83] J. Meyer-ter-Vehn *et al.*, Phys. Fluids B **2**, 1313 (1990).